Environment International 141 (2020) 105714

Contents lists available at ScienceDirect

Environment International

journal homepage: www.elsevier.com/locate/envint

Size resolved aerosol respiratory doses in a Mediterranean urban area: From PM_{10} to ultrafine particles

Maurizio Manigrasso[a,*], Francesca Costabile[b], Luca Di Liberto[b], Gian Paolo Gobbi[b], Maurizio Gualtieri[c], Gabriele Zanini[c], Pasquale Avino[d]

[a] Department of Technological Innovations, INAIL, Via IV Novembre 144, I-00187 Rome, Italy
[b] CNR-ISAC – Italian National Research Council, Institute of Atmospheric Science and Climate, via Fosso del Cavaliere 100, I-00133 Rome, Italy
[c] ENEA SSPT-MET-INAT, Via Martiri di Monte Sole 4, I-40129 Bologna, Italy
[d] Department of Agricultural, Environmental and Food Sciences (DiAAA), University of Molise, via F. De Sanctis, I-86100, Campobasso, Italy

ARTICLE INFO

Keywords:
PM_{10}
Ultrafine particles
Respiratory doses
Olfactory bulb
Combustion
Saharan dust
Sea salt aerosol

ABSTRACT

In the framework of the 2017 "carbonaceous aerosol in Rome and Environs" (CARE) experiment, particle number size distributions have been continuously measured on February 2017 in downtown Rome. These data have been used to estimate, through MPPD model, size and time resolved particle mass, surface area and number doses deposited into the respiratory system. Dosimetry estimates are presented for PM_{10}, $PM_{2.5}$, PM_1 and Ultrafine Particles (UFPs), in relation to the aerosol sources peculiar to the Mediterranean basin and to the atmospheric conditions. Particular emphasis is focused on UFPs and their fraction deposited on the olfactory bulb, in view of their possible translocation to the brain. The site of PM_{10} deposition within the respiratory system considerably changes, depending on the aerosol sources and then on its different size distributions. On making associations between health endpoints and aerosol mass concentrations, the relevant coarse and fine fractions would be more properly adopted, because they have different sources, different capability of penetrating deep into the respiratory system and different toxicological implications. The separation between them should be set at 1 μm, rather than at 2.5 μm, because the fine fraction is considerably less affected by the contribution of the natural sources. Mass dose is a suitable metric to describe coarse aerosol events but gives a poor representation of combustion aerosol. This fraction of particles, made of UFPs and of accumulation mode particles (mainly with size below 0.2 μm), is of high health relevance. It elicited the highest oxidative activity in the CARE experiment and is properly described by the particle surface area and by the number metrics. Such metrics are even more relevant for the UFP doses deposited on the olfactory bulb, in consideration of the role recognized to oxidative stress in the progression of neurodegenerative diseases. Such metrics would be more appropriate, rather than PM_x mass concentrations, to correlate neurodegenerative pathologies with aerosol pollution.

1. Introduction

Atmospheric Particulate Matter (PM) can be described by two main modes, according to their aerodynamic diameter (d_a): a coarse mode (d_a = 10–2.5 μm) and a fine one (d_a < 2.5 μm), that includes ultrafine (d_a < 0.1 μm) and accumulation mode particles (0.1–1 μm). This separation is important because not only fine and coarse mode particles differ in size, but they also differ in chemical composition, and more in general in the formation process. Fine particles are associated to the physicochemical processing of compounds also resulting from anthropogenic sources, mainly combustion sources and may derive form from gas to particle conversion processes. Coarse particles come from processes involving mechanical energy such as the resuspension of deposited dust. The impact on human health of the two classes of particles is different, due to both their different capabilities of penetrating into the respiratory system and their different features (e.g., their different chemical compositions, physical state). Indeed, PM atmospheric pollution has been linked to a range of adverse health outcomes, including carcinogenic effects (IARC, 2013). Specifically, increased PM_{10} concentrations have been associated to increased mortality rates and hospital admissions due to cardiovascular causes (Martuzzi et al., 2002), have been put in relation with bronchitis and asthma exacerbation in adults and children (Romeo et al., 2006; Hoek et al., 2012; WHO, 2013) and with increased risk of hospital admission

* Corresponding author.
E-mail address: m.manigrasso@inail.it (M. Manigrasso).

https://doi.org/10.1016/j.envint.2020.105714
Received 28 December 2019; Received in revised form 25 February 2020; Accepted 1 April 2020
Available online 13 May 2020

Abbreviations

H	head region of the respiratory system
TB	tracheobronchial region of the respiratory system
Al	alveolar region of the respiratory system
R	regions of the respiratory system (H, TB, Al) and olfactory bulb
$D^R(d_{ai}, t)$	aerosol number regional dose as function of time and of aerodynamic diameter
$S^R(d_{ai},t)$	aerosol surface area regional dose as function of time and of aerodynamic diameter
$M^R(d_{ai},t)$	aerosol mass regional dose as function of time and of aerodynamic diameter
$NPM_{10}^R(t)$	total aerosol (from 0.009 μm to 10 μm) number regional doses
$SPM_{10}^R(t)$	total aerosol (from 0.009 μm to 10 μm) surface area regional doses
$PM_{10}^R(t)$	total aerosol (from 0.009 μm to 10 μm) mass regional doses
$D^{Olf}(t)$	total particle number doses deposited on the olfactory bulb upon inhalation
$S^{Olf}(t)$	total particle surface area doses deposited on the olfactory bulb upon inhalation
$NPM_x^R(t)$	PM_x (x = 2.5 μm, 1 μm, 0.1 μm) number regional doses
$SPM_x^R(t)$	PM_x (x = 2.5 μm, 1 μm, 0.1 μm) surface area regional doses
$PM_x^R(t)$	PM_x (x = 2.5 μm, 1 μm, 0.1 μm) mass regional doses
$NPM_{10}^{Tot}(t)$	total aerosol (from 0.009 μm to 10 μm) number doses deposited into the respiratory system
$SPM_{10}^{Tot}(t)$	total aerosol (from 0.009 μm to 10 μm) surface area doses deposited into the respiratory system
$PM_{10}^{Tot}(t)$	total aerosol (from 0.009 μm to 10 μm) mass doses deposited into the respiratory system
$NPM_{10}^{Tot}(\Delta t)$	total cumulative particle number dose deposited into the respiratory system over 1 h-time interval
$SPM_{10}^{Tot}(\Delta t)$	total cumulative particle surface area dose deposited into the respiratory system over 1 h-time interval
$PM_{10}^{Tot}(\Delta t)$	total cumulative particle mass dose deposited into the respiratory system over 1 h-time interval
B	breathing frequency
t	time
d_{ai}	aerodynamic diameter of the ith aerosol size class
d_m	electrical mobility diameter
d_{ve}	equivalent volume diameter
C_c	Cunningham slip factor
$C(d_{ai}, t)$	average 5 min aerosol concentration as function of size and time
$F^R(d_{ai}, t)$	particle regional deposition fraction as function of particle size and residence time within H, TB, Al regions
$F^R_{nearly\ hydrophobic}$	regional deposition fractions of nearly hydrophobic particles
$F^R_{less\ hygroscopic}$	regional deposition fractions of less hygroscopic particles
$F^R_{more\ hygroscopic}$	regional deposition fractions of more hygroscopic particles
α	number fraction of nearly hydrophobic particles
β	number fraction of less hygroscopic particles
γ	number fraction of more hygroscopic particles
V_t	tidal volume
ρ_0	reference density (1 g cm^{-3})
ρ	particle density
χ	particle dynamic shape factor
$G_{f\text{-}90}$	90% RH hygroscopic grow factors
$G_{f\text{-}99.5}$	99.5% RH hygroscopic grow factors
$d_a(0)$	initial dry aerodynamic diameter
$d_a(\infty)$	equilibrium aerodynamic diameter at 99.5% RH
RH%	percent relative humidity
PBL	Planetary Boundary Layer
UFPs	ultrafine particles
ROS	Reactive Oxygen Species

for ischemic stroke (Wellenius et al., 2005).

Stronger associations between PM and mortality have emerged when $PM_{2.5}$ has been considered rather than PM_{10} (Dockery et al., 1993; Levy et al., 2000; WHO, 2013). In 2016, 95% of the world's population lived in areas with $PM_{2.5}$ concentrations above the World Health Organization 10 μg m^{-3} (annual average) guideline (Shaddick et al., 2018).

Pope et al. (2002) observed that 10 μg m^{-3} increments of $PM_{2.5}$ were associated with increased risk of all-cause, cardiopulmonary and lung cancer mortality respectively of about 4%, 6% and 8% in metropolitan areas in the United States. The same association was found by Lepeule et al. (2012) who reported increased risk of all-cause mortality, cardiovascular and lung-cancer mortality respectively of 14%, 26% and 37%, with a concentration-response relationship linear down to $PM_{2.5}$ concentrations of 8 μg m^{-3}. Coherently, it is in the fine fraction of PM that toxicologically relevant components such as polycyclic aromatic hydrocarbons (PAH), nitrated and oxygenated PAH derivatives (Avino et al., 2002; Avino and Manigrasso, 2008; Albinet et al., 2008; Di Filippo et al., 2015) and Black Carbon (Avino et al., 2000; Viidanoja et al., 2002; Targino et al., 2016) are retrieved, together with metals, that are distributed both in the coarse and in fine aerosol (Shi et al., 2014; Fang et al., 2017). As to the adverse health effects sulfates, that are also a component of the fine fraction, Pope et al. (2007) reported that a 2.5-μg m^{-3} decrease over an 8.5-month period, was associated with a 2.5% decrease in the number of deaths. On the other hand, Smith et al. (2009) addressed the discrepancies between toxicological and epidemiological studies. The first, using pure sulfates, have found negligible effects, whereas the second, referring to particle-phase sulfates, probably because in mixture with other components, have found significant associations. In agreement with that was the study of Fang et al. (2017) who proposed the mechanism of metals dissolution due to highly acidic sulfate aerosol and the relevant effect on particle oxidative potential, possibly explaining the sulfate-health associations reported by other studies. More recently the attention has been focused on the smaller PM_1 fraction. Lin et al. (2016) reported that the cardiovascular mortality in Guangzhou (China) was significantly associated with PM_{10}, $PM_{2.5}$ and PM_1, with no significant effect due to $PM_{2.5\text{-}10}$ and $PM_{1\text{-}2.5}$. Therefore, the authors argued that the cardiovascular effects of PM_{10} and $PM_{2.5}$ were possibly explained by PM_1. Other studies as well did not find any statistically significant associations between $PM_{2.5\text{-}10}$ and daily mortality (Peng et al., 2008; Chen et al., 2011). However, this does not mean that the coarse fraction of PM is devoid of any health effect (Sandström et al., 2005). Indeed, Brunekreef and Forsberg (2005) pointed out that in studies of chronic obstructive pulmonary disease, asthma and respiratory admissions, the short-term effect of coarse PM is stronger, or as strong as $PM_{2.5}$ effect. Zanobetti and Schwartz (2009) reported a strong association of both fine and coarse particles with daily deaths. Malig and Ostro (2009) as well found an association between acute exposure to coarse particles and all-cause and cardiovascular mortality.

A source of coarse dust in the area of the Mediterranean basin is represented by Saharan dust advections (Querol et al., 2009; Manigrasso et al., 2012; Gobbi et al., 2019). Gobbi et al. (2013) reported that Saharan dust advected over Rome on 30% of the days of 2001, with a mean contribution to daily PM_{10} of about 15.6 μg m^{-3}. Regarding the health effects of desert dust, Perez et al. (2008) reported

that during Saharan dust days in Barcelona, a daily increase of 10 μg m^{-3} of $PM_{10-2.5}$ was associated with a daily mortality increase of 8.4% compared with 1.4% during non-Saharan dust days. The authors speculated that such effects might have been possibly due to biogenic components and to other chemicals transported with the $PM_{10-2.5}$ fraction. In agreement with that, Mallone et al. (2011) found effects of $PM_{2.5-10}$ and PM_{10} on cardiac and circulatory mortality during Saharan dust episodes in Rome, stronger than in no-dust days. Salvadora et al. (2019) explained such effects proposing a synergistic action of local pollutants and mineral dust accumulating, due to a reduction of the mixing layer height.

On the other hand, Meng et al. (2013) emphasized the role of fine mode particles and observed that particles < 0.5 μm in diameter may be most responsible for adverse health effects of particulate air pollution and that adverse health effects may increase with decreasing particle size. Indeed, Ultrafine Particles (UFPs, particles sized < 0.1 μm) are small compared to cellular structure (Avino et al., 2016; Manigrasso et al., 2019a), their number concentrations and surface areas are high, so that organic molecules can be adsorbed onto them and can efficiently penetrate into the lung, systemic circulation and cellular targets, inducing oxidative stress (Donaldson et al., 2001; Li et al., 2003).

Evidence of association between combustion-related ultrafine particles and the oxidative response in the human body was just reported by Costabile et al. (2019). Recently a growing concern has risen on the clinical effects of atmospheric pollution on the central nervous system (Babadjouni et al., 2017), with significant agreement between epidemiological and animal studies, with the support of in vitro studies as to an increased oxidative stress and neuroinflammation mechanism (Costa et al., 2014). Calderón-Garcidueñas et al. (2004, 2008, 2012) have proposed that UFPs may possibly play a role in the etiology of neurodegenerative diseases, such as Alzheimer's disease. Coherently, Chen et al. (2017), in a population-based cohort study, reported adjusted hazard ratios of incident dementia of 1.07, 1.04, 1.02, 1.00 for people living respectively < 50 m from a major traffic road, for 50–100 m, for 101–200 m, and for 201–300 m versus further than 300 m.

Several studies have demonstrated the translocation to brain through olfactory bulb and olfactory nerve of intranasally instilled (Oberdörster et al., 2005; Manigrasso et al., 2019b) and inhaled nanoparticles in experiment animals (Oberdörster et al., 2004; Balasubramanian et al., 2013). Recently Maher et al. (2016) reported the presence in the human brain of combustion-derived magnetite and of other metal-bearing nanoparticles.

In addition, in vitro test results clearly show the capability of coarse, fine and ultrafine particles to activate significant biological responses after exposure (Gualtieri et al., 2018). Different PM fractions have been shown to activate specifically selected biological pathways; nonetheless, the main mechanisms defined are oxidative stress, genotoxicity, and inflammation. These mechanisms, also by an interplay among them are able to impair the normal cellular physiological/biochemical processes and, in the long term, result in significant tissues damages which might improve the onset of the adverse health outcomes reported by epidemiological and clinical incidence data.

From this context, the need emerges to measure and regulate all the PM size fractions, from UFPs to coarse PM, since all of them entail acute and/or chronic adverse effects on human health. In this perspective, size resolved aerosol measurements represent a relevant task, because they allow to estimate the doses of particles deposited in the regions of the respiratory system and directly correlate with health effects.

With this purpose, in the framework of the 2017 Carbonaceous Aerosol in Rome and Environs (CARE) experiment (Costabile et al., 2017) particle number size distributions have been continuously measured on February 2017 in downtown Rome. Based on these data, aerosol doses deposited in the head (H), tracheobronchial (TB) an alveolar (Al) regions of the human respiratory system (Manigrasso et al., 2018) have been estimated, together with the doses deposited upon inhalation, on the olfactory bulb. The main goal of this paper is therefore to provide modelling information on the relevance of different PM fractions on the possible doses (in mass, surface area and number) deposited at different target sites, adding relevant information for future set up/interpretation of epidemiological, clinical and toxicological studies.

2. Materials and methods

2.1. Aerosol measurements

Aerosol measurements were performed on February 2017 at the "San Sisto" garden, an urban background site in downtown Rome. This urban background site is entoured by three traffic roads approximately 100–800 m away from them (Fig. S1 of Supplementary Material).

The particle number size distribution from 0.0088 to 10 μm was measured with 5 min time resolution by coupling a Scanning Mobility Particle Sizer (TROPOS SMPS, Wiedensohler et al., 2012) equipped with a butanol-based Condensation Particle Counter (CPC, model 3772, TSI) in the particle size range from 8.8 to 800 nm (electrical mobility diameter), with and an Aerodynamic Particle Sizer (APS, model 3321, TSI) in the particle size range from 0.5 to 10 μm (aerodynamic diameter). SMPS data were corrected for penetration errors through the sampling line, penetration efficiency due to diffusion losses (Hinds, 1999) being higher than 98.92% for particles bigger than 15 nm, and merged to APS number size distributions according to the algorithm of Khlystov et al. (2004), as reported by Costabile et al. (2017) and Alas et al. (2019). All the instruments were operated within the AEROLAB mobile laboratory (http://www.isac.cnr.it/en/content/aerolab).

2.2. Dosimetry evaluation

Aerosol number regional doses $D^R(d_{ai},t)$, as function of time (t) and of the aerodynamic diameter (d_{ai}), were estimated as the number of particles deposited during the APS + SMPS measuring time interval (5 min), in the head (H, nose, larynx, pharynx and mouth; ICRP, 1994), tracheobronchial (TB) and alveolar (Al) regions and on the olfactory bulb (Olf) according to Eq. (1). During such time interval, the particle number concentrations $C(d_{ai},t)$ were supposed to be constant.

$$D^R(d_{ai}, t) = 5B \times C(d_{ai}) \times F^R(d_{ai}, t) \times V_t \mathrm{R} = \mathrm{H, TB, Al, Olf} \quad (1)$$

B is the breathing frequency (min^{-1}), V_t is the tidal volume, $F^R(d_{ai},t)$ is the particle regional deposition fraction, d_{ai} is the particle aerodynamic diameter of particles classified in the i^{th} size channel of the APS + SMPS measuring system. Since SMPS measures aerosol size number distribution as a function of the electrical mobility diameter (d_m), d_m values were transformed into aerodynamic diameter (d_a) according to Eq. (2) (Khlystov et al, 2004).

$$d_a = d_m \sqrt{\frac{1}{\chi} \times \frac{\rho \times C_c(d_m)}{\rho_0 C_c(d_a)}} \quad (2)$$

where χ is the particle dynamic shape factor. X as a function of aerodynamic diameter was estimated by interpolating, through the Akima (1970) algorithm, the data reported by Hu et al. (2012) in the range from 0.1 to 1.8 μm in Beijing. For d_a outside this range the relevant lower bound and upper bound χ values were adopted (1.13 for d_a < 0.1 μm and 1 for d_a > 1.8 μm).

ρ_0 is the standard density (1 g cm^{-3}). ρ is the particle density as a function of aerodynamic diameter, estimated by interpolating (Akima, 1970) the density data reported in Costabile et al. (2017). Cc is the Cunningham slip factor for a given diameter.

Aerosol number concentrations were measured as function of the dry aerodynamic diameter (APS data) and of dry electrical mobility diameters (SMPS), by keeping the RH in the sampling line always below 30%. Relative humidity (RH%) in the respiratory system is near to saturation (ICRP, 1994), therefore, particles once entered in the

respiratory system may undergo hygroscopic growth in relation to their hygroscopicity. As a result of that, their sizes increase, and the relevant deposition fractions change. Particle hygroscopic grow factors, defined as the ratio between humidified and dry diameters at a given RH%, allow to account for such particle size variation. To this purpose, we adopted the size resolved 90% RH hygroscopic grow factors ($G_{f\text{-}90}$) reported by Swietlicki et al. (2008) and by Stock et al. (2011). These authors considered three hygroscopic growth groups (nearly hydrophobic, less hygroscopic, more hygroscopic). Within each hygroscopic group considered by these authors, we took the average $G_{f\text{-}90}$ value for each dry diameter considered and interpolated the so obtained data set with a 5th grade polynomial, in order to obtain the relevant $G_{f\text{-}90}$ values for the particle size explored by the SMPS + APS measuring system.

99.5% RH hygroscopic grow factors ($G_{f\text{-}99.5}$) were calculated, according to Vu et al. (2015), with Eq. (3), where d_p is the particle dry diameter:

$$G_{f-99.5} = \sqrt[3]{1 + (G_{f-90}^3 - 1).\ \frac{99.5}{90}.\ \frac{\left(\frac{2.09}{100e^{dp.G_{f-90}} - 90}\right)}{\left(\frac{2.09}{100e^{dp.G_{f-99.5}} - 99.5}\right)}} \quad (3)$$

Particle hygroscopic growth as a function of the residence time (t) within the regions of the respiratory system has been estimated by means of Eq. (4) (ICRP, 1994):

$$d_a(t) = d_a(\infty) - [d_a(\infty) - d_a(0)] \times \left\{exp\left[\frac{-(10t)^{0.55}}{d_a(0)}\right]\right\}^{0.6} \quad (4)$$

where $d_a(0)$ is the initial dry aerodynamic diameter and $d_a(\infty)$ is the equilibrium aerodynamic diameter:

$$d_a(\infty) = G_{f-99.5} \times d_a(0) \quad (5)$$

The particle regional deposition fractions ($F^R(d_{ai})$) were estimated using the Multiple-Path Particle model Dosimetry (MPPD v3.01, ARA 2015, ARA, Arlington, VA, USA) (Asgharian et al., 2001; Manigrasso et al., 2017). The 60th percentile human stochastic lung was considered along with the following settings: (i) a uniformly expanding flow, (ii) an upright body orientation, and (iii) nasal breathing with a 0.5 inspiratory fraction and no pause fraction. Moreover, the following parameters were used for a Caucasian adult male under light work physical activity, based on the ICRP report (ICRP, 1994): (i) a functional residual capacity (FRC) of 3300 mL, (ii) an upper respiratory tract (URT) volume equal to 50 mL, (iii) a 20 min^{-1} breathing frequency, and (iv) an air volume inhaled during a single breath (tidal volume, V_t) of 1.25 L.

For each APS + SMPS ith size channel $F^R(d_{ai})$ was calculated through Eq. 6 (Vu et al., 2015):

$$F^R(d_{ai}, t) = \alpha F^R_{nearly\ hydrophobic}(d_{ai}, t) + \beta F^R_{less\ hygroscopic}(d_{ai}, t) + \gamma F^R_{more\ hygroscopic}(d_{ai}, t) \quad (6)$$

$F^R_{nearly\ hydrophobic}$, $F^R_{less\ hygroscopic}$, $F^R_{more\ hygroscopic}$ are the deposition fractions of nearly hydrophobic, less hygroscopic, more hygroscopic particles respectively. α, β, γ are the relevant number fractions (α + β + γ = 1). They were estimated by interpolating (Akima, 1970) the data of Ye et al. (2013), Massling et al. (2009) and Stock et al. (2011), in the range 30–1200 nm. For particle sizes below and above such range, respectively, the lower and the upper interval bounds α, β, γ values were adopted.

Aerosol mass ($M^R(d_{ai},t)$) and surface area doses ($S^R(d_{ai},t)$) were calculated from aerosol number doses $D^R(d_{ai},t)$, using the density data reported in Costabile et al. (2017) and supposing spherical particles with diameters equal to the particle volume equivalent diameter (d_{ve}). d_{ve} was calculated from electrical mobility diameter according to Eq. (7) (DeCarlo et al., 2004):

$$\frac{d_m}{C_c(d_m)} = \frac{d_{ve} \times \chi}{C_c(d_{ve})} \quad (7)$$

Total particle (from 0.009 μm to 10 μm) number regional doses ($NPM^R_{10}(t)$) were calculated according Eq. (8):

$$NPM^R_{10}(t) = \sum_{0.009\mu m}^{10\mu m} D^R(d_{ai}, t) \quad (8)$$

Total particle surface regional doses ($SPM^R_{10}(t)$) and total particle mass regional doses ($PM^R_{10}(t)$) were calculated in the same way from $S^R(d_{ai},t)$ and $M^R(d_{ai},t)$, respectively.

Total particle number doses deposited upon inhalation on the olfactory bulb were estimated as according to Eq. (9):

$$D^{Olf}(t) = \sum_{0.009\mu m}^{10\mu m} D^{Olf}(d_{ai}, t) \quad (9)$$

Total particle surface area doses ($S^{Olf}(t)$) deposited on the olfactory bulb were calculated from $D^{Olf}(t)$ (Eq. (9)), supposing spherical particles.

PM_x (x = 2.5 μm, 1 μm, 0.1 μm) regional doses ($NPM^R_x(t)$, $SPM^R_x(t)$, $PM^R_x(t)$) were calculated carrying out the summation of Eq. (8) up to 2.5 μm, 1 μm and 0.1 μm (UFPs).

Total particle doses deposited in the respiratory system, $NPM^{Tot}_{10}(t)$, $SPM^{Tot}_{10}(t)$, $PM^{Tot}_{10}(t)$, were calculated as summation of the relevant regional (H, TB, Al) doses.

Total cumulative particle number doses deposited into the respiratory system over a time interval (Δt), $NPM^{Tot}_{10}(\Delta t)$, $SPM^{Tot}_{10}(\Delta t)$, $PM^{Tot}_{10}(\Delta t)$ were calculated as summation over a 1 h-time interval (Δt) respectively of $NPM^{Tot}_{10}(t)$, $SPM^{Tot}_{10}(t)$, $PM^{Tot}_{10}(t)$.

2.3. Statistical elaborations

Statistical analyses were carried out on PM_x (x = 2.5 μm, 1 μm, 0.1 μm) regional mass doses $PM^R_x(t)$ by means of IBM-SPSS version 25.0 software (IBM Corp. Released 2017. IBM SPSS Statistics for Windows, Version 25.0. Armonk, NY: IBM Corp.). The Kolmogorov-Smirnov test was used to assess the normality of the distribution. $PM^R_{10}(t)$ exhibited a not normal distribution, thus non-parametric tests were used for statistical evaluations. Kruskal-Wallis test was used with pairwise post-hoc tests to evaluate the differences in median $PM^R_{10}(t)$ levels.

3. Results and discussion

3.1. Overview of the field measurement

Detailed descriptions of the aerosol sources, physicochemical properties and related in-vitro and in vivo biological responses are reported in previous papers (Costabile et al., 2017; Gualtieri et al., 2018; Nava et al., 2018; Costabile et al., 2019; Alas et al., 2019; Valentini et al., 2020; Fiorello et al., 2020). Briefly, in relation to the atmospheric conditions and aerosol pollution sources, the measuring campaign, can be classified in three different periods peculiar to urban areas of the Mediterranean basin:

1) The period from February the 1st to February the 6th was characterized by unstable weather conditions: strong winds from E-SE, high values of the momentum fluxes and turbulent kinetic energy (TKE), low natural radioactivity due to the Radon progeny and some rain on 05th–06th (Costabile et al., 2017) This favoured relatively low aerosol concentration. On February the 4th and 5th a clear event of marine aerosol advection occurred (Nava et al., 2018).
2) The period from February the 10th to February the 24th (with the exclusion of 18th–19th) was characterized by fairly stable weather conditions with the typical local winter circulation (weak sea breezes). This favoured the increase of aerosol mass concentrations from local sources. A source apportionment study revealed the

predominance of three aerosol sources (Costabile et al., 2019). The biomass burning aerosol occurred mainly during the nocturnal hours, with particles in the sub-micrometer size range enriched in organic aerosol. Fresh traffic related aerosol occurred during the rush hours, with particles in the ultrafine particle size range (manly below 20 nm) enriched in black carbon. A coarse mode aerosol was also observed. Higher concentration of the sulfate aerosol were found from the 12th to the 18th and from the 21st to the 25th (Nava et al., 2018).

3) The period from February the 24th to the 26th was characterized by unstable weather conditions, higher wind speeds from E-SE, the advection of Saharan dust, which reached the ground, and some sulfate aerosol (Costabile et al., 2017; Nava et al., 2018).

Dosimetry estimates were carried out for each day of the measuring campaign. February 4th, 16th and 24th-25th were selected as representative for a detailed description of periods 1), 2) and 3), respectively. The 16th of February was characterised by a significant expression of genes belonging to the antioxidant responsive element and in-vivo and in-vitro oxidative responses higher than the 24th of February, which presented no significant biological response (Gualtieri et al., 2018; Costabile et al., 2019). No consistent biological finding has been found for the 4th of February.

3.2. Dosimetry data

3.2.1. Particle mass doses

Fig. 1 shows the temporal evolution of total particle mass ($PM_{10}^{R}(t)$) regional doses on February 4th, 16th, 24th and 25th. Higher $PM_{10}^{R}(t)$ doses were deposited in the head than in the TB and Al regions. This occurs because UFPs efficiently penetrate into the alveolar region and are numerically more abundant, whereas their mass is relatively negligible, in comparison with particles of greater size that preferentially deposit into the head region, accounting for as much as 75–90% of the total aerosol mass deposited into the respiratory system.

The temporal trend of $PM_{10}^{R}(t)$ on 16th was mainly determined by combustion sources (Costabile et al., 2017). Biomass burning aerosol was present between 12 am and 10 am, with particular relevance between 12 am and 4 am, and between 8 pm and 12 pm. Fresh traffic aerosol was present between 6 am and 12 pm and between 4 pm and 9 pm. Following the intensity of the emission sources and the Planetary Boundary Layer (PBL) modulation a clear minimum was observed in the central hours of the day (12 pm–4 pm).

On February 4th the $PM_{10}^{R}(t)$ minimum in the central part of the day was not present, instead, a slightly increasing trend was observed, due to the advection of sea salt aerosol favoured by the meteorological conditions of period 1 days (high wind speed).

From midday of 24th until 26th (period 3 days) PBL mixing height became higher (lower natural radioactivity) in comparison with the days of period 2. Advected Sharan dust reached the ground and clearly influenced $PM_{10}^{R}(t)$. $PM_{10}^{R}(t)$ presented a broad maximum starting from about 1 pm of 24th and ending at about 6 am of 25th.

For each hour of outdoor exposure Total cumulative particle mass doses ($PM_{10}^{Tot}(\Delta t)$) of 2.5×10^4–4.9×10^4 ng, 1.4×10^4–6.2×10^4 ng, 9.8×10^3–2.9×10^4 ng and 8.4×10^3–7.2×10^4 ng were deposited into the respiratory system, respectively on February 4th, 16th, 24th and 25th. The relevant temporal trend is shown in Fig. S2a of the Supplementary Material. On period 2 days (atmospheric stability), maximum $PM_{10}^{Tot}(\Delta t)$ were observed at the beginning and at the end of the day, rather than at the traffic rush hours. This is due to the relative contribution of accumulation mode particles (0.1–1.0 μm), that to a greater extent contribute to particle mass and surface area and increase over UFPs in periods distant from traffic congestion. The contribution of sea salt aerosol on 04th was clearly seen between 01 pm and 08 pm, when $PM_{10}^{Tot}(\Delta t)$ was higher than on 16th, notwithstanding the stable atmospheric conditions favouring pollutant accumulation, on 16th.

On days of period 3, $PM_{10}^{Tot}(\Delta t)$ was markedly influenced by the advection of Saharan dust and by the modulation of PBL mixing height: desert dust is transported from remote areas at high altitudes, so that the vertical remixing of the lower troposphere allows it to mix with surface aerosol. The temporal evolution of aerosol mass size distribution $M^{R}(d_{ae},t)$ on February 04th, 16th, 24th and 25th, in connection with the emission sources is described in Supplementary material (Figs. S3 and S4).

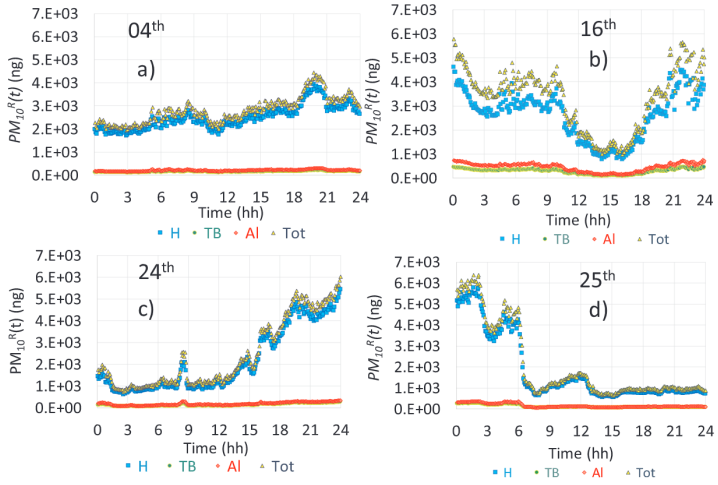

Fig. 1. Temporal evolution of total particle mass ($PM_{10}^{R}(t)$) regional doses (R = H, TB, Al, Tot) on February 4th (a), 16th (b), 24th (c) and 25th (d), 2017. Each data point represents the dose deposited in a 5 min time interval.

Fig. 2 shows the temporal trend of the percent contribution of $PM_x^R(t)$ to $PM_{10}^R(t)$ on 4th, 16th, 24th and 25th. The relevant ranges of variation are summarized in Table 1. As a general trend, the percent contributions of $PM_{2.5}^R(t)$ and of $PM_1^R(t)$ (t) doses increased passing from the H to the TB and alveolar regions, because of the filtering action of the nasopharyngeal passages and of the mouth cavity.

In detail, the percent contribution of $PM_{2.5}$ deposited in the H and the TB regions was higher on 16th (Fig. 2d and e) than on 4th (Fig. 2a and b), denoting a significant contribution of the coarse fraction.

The difference of $PM_{10}^R(t)$ between the two days was even more striking if seen in terms of PM_1, on 16th a great percentage of PM_{10} deposited in the H region was made of PM_1 (Fig. 2d). The difference between the two fractions was even more reduced in the TB region (Fig. 2e) and in the Al region (Fig. 2f), where PM_{10} was almost completely represented by PM_1. On the contrary, on 04th (Fig. 2a–c) not only the percent contribution of $PM_1^R(t)$ to $PM_{10}^R(t)$ was considerably lower but there was also a marked difference between $PM_1^R(t)$ % and $PM_{2.5}^R(t)$ % explainable considering the contributions of sea salt aerosol

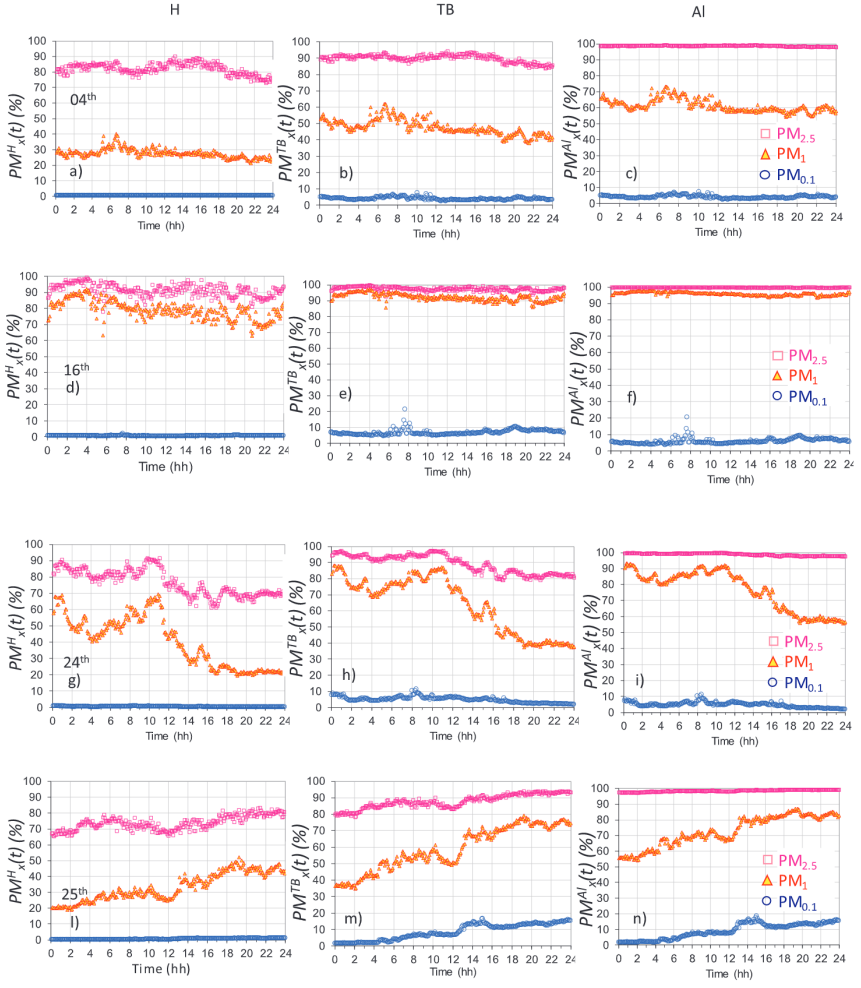

Fig. 2. Temporal trends of the percent contribution to total particle mass regional doses ($PM_{10}{}^R$(t)) of the mass based $PM_x{}^R$(t) (line colors represent x = 2.5 μm, 1 μm, 0.1 μm; column address R = H, TB, Al) on February 04th (a, b, c), 16th (d, e, f), 24th (g, h, i)and 25th (l, m, n). Each data point refers to a 5-min time interval.

Table 1
Ranges of variation of the percent contribution to total particle mass regional doses ($PM_{10}{}^{R}(t)$) of the mass based $PM_x{}^{R}(t)$ (x = 2.5 μm, 1 μm, 0.1 μm), referred to a 5-min time interval, on February 04th, 16th, 24th and 25th.

Day	$PM_{2.5}^{H}(t)$(%)	$PM_{1}^{H}(t)$(%)	$PM_{0.1}^{H}(t)$(%)	$PM_{2.5}^{TB}(t)$(%)	$PM_{1}^{TB}(t)$(%)	$PM_{0.1}^{TB}(t)$(%)	$PM_{2.5}^{Al}(t)$(%)	$PM_{1}^{Al}(t)$(%)	$PM_{0.1}^{Al}(t)$(%)
4th	72.8–90.0	21.3–40.2	0.1–0.4	83.7–94.2	37.8–62.0	2.3–7.3	97.9–99.2	54.3–73.2	2.2–7.1
16th	78.1–99.3	63.2–92.3	0.4–2.0	92.5–99.8	85.5–97.0	4.2–21.4	99.3–99.9	93.6–97.7	3.4–20.6
24th	61.3–91.5	19.4–69.2	0.1–0.9	78.9–97.3	37.3–88.1	1.6–11.3	97.5–99.7	55.6–93.2	1.7–11.2
25th	65.4–83.6	19.1–52.1	0.1–1.2	78.6–94.3	35.0–79.3	1.5–16.8	97.3–99.4	54.4–87.1	1.7–18.5

and on period 1 days. Such contribution was lacking on period 2 days when $PM_{10}^{R}(t)$ was almost made of submicron combustion aerosol.

On the 24th and 25th of February (Fig. 2g–n) the differences between PM_{10} and $PM_{2.5}$ doses were even more marked due to the influence of coarse Saharan dust on surface aerosol. The contribution of $PM_{2.5}^{R}(t)$ to $PM_{10}^{R}(t)$ in the H and TB regions was markedly lower than on 16th and the coarse fraction became negligible only in the Al region.

Moreover, in contrast to period 2 days, due to the contribution of desert dust, $PM_{2.5}^{R}(t)$ was no more almost completely explained by $PM_{1}^{R}(t)$. This occurred not only in the H region, where the difference between the two fractions became as high as 50%, but also in the TB and Al regions, where the differences between the two fractions was as high as 45% and 42%, respectively.

The mass contribution of UFPs to $PM_{10}^{R}(t)$ ($PM_{0.1}^{R}(t)$%) was negligible. This was particularly evident in the H region, whereas in the TB and Al regions the contribution ranged from negligible percentages to below 19%.

Table 2 shows the pairwise post-hoc tests performed together with the Kruskal-Wallis test on $PM_{x}^{R}(t)$ for February 4th, 16th, and 24th, the relevant box plots are reported in Fig. S5 of Supplementary Material. On the 4th there was a statistically significant difference ($p < 0.001$) among the three PM_x fractions deposited in the H an TB regions and in the alveolar region between the pairs PM_1-$PM_{2.5}$ and PM_1-PM_{10}. This is due to the respiratory deposition of coarse particles and of particles with size in between 1 μm and 2.5 μm, deriving from sea salt aerosol advection. On the contrary, there was no statistical difference ($p = 1.000$) between $PM_{2.5}$ and PM_{10} in the Al region. Such occurrence, observed for 16th and 24th as well, is due the removal of the coarse PM fraction operated by the H and the TB regions.

On the 16th such a filtrating action was already effective in the TB region, because on that day PM10 was almost made of fine mode aerosol due to local combustion sources. In the Alveolar region, there was no statistically significant difference among the three fractions: PM_{10} particles was almost represented by submicron particles.

On the second half of the 24th, surface aerosol was markedly influenced by the advection of Saharan dust, whose size distribution extends down below 1 μm, with peak in the 2.5 μm diameter range (Gobbi et al., 2019). As a result of that, PM_{10}, $PM_{2.5}$ and PM_1 doses were statistically different down to the tracheobronchial region, and in the alveolar region, with the exception of PM_{10} vs. $PM_{2.5}$.

3.2.2. Particle surface area doses

The temporal evolution of total particle surface ($SPM_{10}^{R}(t)$) regional doses $SPM_{10}^{R}(t)$) (Fig. 3) was the same as $PM_{10}^{R}(t)$ (Fig. 1), being influenced both by the intensity of the aerosol source emissions and by the PBL modulation. However, expressing the doses in the surface area rather than in mass metric affects their distribution in the respiratory system. On mass basis, on average 78–87% of the dose was deposited in the H region. Such percentages, on the surface area metric decreased to 66–73%. Conversely, the particle surface area that reached the TB and Al regions increased respectively by 3–7% and by 6–12%.

For each hour of outdoor exposure Total cumulative particle surface area doses $SPM_{10}^{Tot}(\Delta t)$ of 9.5×10^{7}–1.7×10^{8} μm^2, 1.4×10^{8}–6.0×10^{8} μm^2, 6.9×10^{7}–2.0×10^{8} μm^2, 4.7×10^{7}–2.0×10^{8} μm^2 were deposited into the respiratory system, respectively on the 04th, 16th, 24th, 25th of February 2017. This data are in agreement with those reported in Albuquerque et al. (2012), although here we clearly showed the significant different deposition at different regions of the respiratory tract. The relevant temporal trend is shown in Fig. S2b of Supplementary Material. The highest doses were estimated for the 16th in the periods of the day when biomass burning and traffic combustion sources were more intense, because of the important contribution of accumulation mode particles and of UFPs to the particle surface area doses.

The temporal evolution of aerosol surface area dose size distribution $S^{R}(d_{ai},t)$ on February 04th, 16th, 24th and 25th, in connection with the emission sources is described in Supplementary material (Fig. S6).

Fig. 4 shows the temporal trend of the percent contribution of $SPM_{x}^{R}(t)$ to $SPM_{10}^{R}(t)$ on 04th (a, b, c), 16th (d, e, f), 24th (g, h, i) and 25th (l, m, n). The relevant ranges of variation are summarized in Table 3.

Compared to Fig. 2, based on mass metric ($PM_x{}^{R}(t)$ %), the contribution of the coarse fraction decreased. It was always negligible in the alveolar region and on 16th (local combustion sources) became negligible starting from the H region. On 04th it ranged from about 4% to 10% and from 1% to 3% in the H and TB regions respectively (Fig. 4a,b), due to the contribution of sea salt aerosol. On 24th and 25th it ranged from about 1% to 14% in the H region and from negligible levels to 4% in the TB region, due to Saharan dust. Conversely, the contribution of PM_1 particles increased, with daily average increments over the mass metric of 17–39%, 7–40%, 4–29%, respectively in the H, Tb and Al regions, reflecting the important contribution of

Table 2
Pairwise post-hoc tests performed together with the Kruskal-Wallis test (*p*-values) on $PM_{x}^{R}(t)$ for February 4th, 16th, and 24th.

Day	$PM_x{}^{R}(t)$ (ng)	H			TB			Al		
		PM_1	$PM_{2.5}$	PM_{10}	PM_1	$PM_{2.5}$	PM_{10}	PM_1	$PM_{2.5}$	PM_{10}
4th	PM_{10}	< 0.001	< 0.001	–	< 0.001	< 0.001	–	< 0.001	**0.575**	–
	$PM_{2.5}$	< 0.001	–	< 0.001	< 0.001	–	< 0.001	< 0.001	–	**0.575**
	PM_1	–	< 0.001	< 0.001	–	< 0.001	< 0.001	–	< 0.001	< 0.001
16th	PM_{10}	< 0.001	0.003	–	0.002	**0.353**	–	**0.213**	**0.896**	–
	$PM_{2.5}$	–	–	0.003	0.030	–	**0.353**	**0.211**	–	**0.896**
	PM_1	–	< 0.001	< 0.001	–	0.030	0.002	–	**0.211**	**0.213**
24th	PM_{10}	< 0.001	< 0.001	–	< 0.001	0.014	–	< 0.001	**0.757**	–
	$PM_{2.5}$	< 0.001	–	< 0.001	< 0.001	–	0.014	< 0.001	–	**0.757**
	PM_1	–	< 0.001	< 0.001	–	< 0.001	< 0.001	–	< 0.001	< 0.001

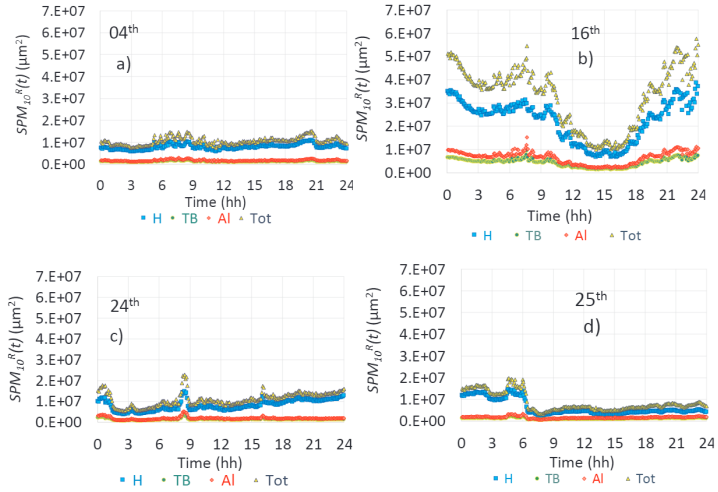

Fig. 3. Temporal evolution of total particle surface area ($SPM_{10}^{R}(t)$) regional doses (R = H, TB, Al, Tot) on 4th (a), 16th (b), 24th (c) and 25th (d). Each data point represents the dose deposited in a 5 min time interval.

accumulation mode particles and of UFPs to the particle surface area metric. UFP doses passed from being completely negligible in the H region, if expressed in mass, to level that ranged, over the four days considered, from 1.4% to 13.0% and increased from the TB (13.7–59.6%) to the Al region (12.9–65.9%) (Table 3). It is worth observing that on 25th, between 12.00 and 16.00, $SPM_{0.1}{}^{R}(t)\%$ reaches values of about 60% in the TB and Al region. Such increasing trend has been observed in Fig. 2, as well.

Several studies have addressed the relationship between particle surface area and health adverse outcomes (Oberdörster et al., 2005; Albuquerque et al., 2012; Hennig et al., 2018). Such effects have been associated to the ability of inhaled particles to generate Reactive Oxygen Species (ROS) on their surface. In particular, UFPs, compared with larger-sized particles of the same chemical composition, can generate higher levels of ROS, due to their higher surface area per unit mass and to their surface reactivity (Oberdörster et al., 2005; Hussain et al., 2009). ROS generation has been addressed as one of the main features explaining toxic effects of inhaled engineered NPs and environmental ultrafine particles (Nel et al., 2006), such as oxidative DNA damage, unregulated cell signalling changes in cell motility, cytotoxicity and apoptosis (Nel et al., 2006; Xia et al., 2008; Zhu et al., 2013).

3.2.3. Particle number doses

Fig. 5 describes the temporal trend of total particle number ($NPM_{10}^{R}(t)$) regional doses on 4th, 16th, 24th and 25th. Compared to $PM_{10}^{R}(t)$ (Fig. 1), some important changes can be noticed. On number basis, the greatest fraction of the doses was deposited in the Al region instead of in the H region (Fig. 1). On average, over the four days considered $NPM_{10}^{H}(t)\%$, $NPM_{10}^{TB}(t)\%$ and $NPM_{10}^{Al}(t)\%$ were in the range respectively of 19–20%, 25–27%, 48–54%.

On 4th (Fig. 5a) the slightly increasing trend observed in the central part of the day for $PM_{10}^{R}(t)$), due to the advection of sea salt aerosol (Fig. 1a), was no more detectable. On February 24th and 25th (Fig. 5c and d) the important contribution of Saharan dust to the mass doses (Fig. 1c and d) was hardly visible in number doses. All these changes derive from the fact that UFPs have low mass but are highly represented in number metric.

Moreover, on the 25th at about 8 am, when the PBL mixing height increased, $NPM_{10}^{R}(t)$ started increasing, instead of decreasing, as would have been the case for a higher dilution. This was due to the nucleation of new particles from the gas phase. Such episodic observation is an issue that deserves further investigation on whether it could represent a concurrent hypothesis to explain the health effects observed during Saharan dust advection events. Such episode is more in detail discussed in the Supplementary Material (Fig. S7).

Fig. S2c of Supplementary Material shows the 1-h cumulative dose daily trends, $NPM_{10}^{Tot}(\Delta t)$. The highest doses were estimated for 16th (6.5×10^{9}–2.4×10^{10} particles), due to the stable atmospheric conditions. On the contrary, at the end of 24th and at the beginning of 25th, the PBL enhancement caused the dilution of local fine combustion aerosol, consequently $NPM_{10}^{Tot}(\Delta t)$ markedly decreased (about 2.0×10^{9} particles).

Conversely, since desert dust is transported from remote areas at high altitudes, the vertical remixing of the lower troposphere allows it to mix with surface aerosol. This is the reason why the $NPM_{10}^{Tot}(\Delta t)$ decrease (Fig. S2c of Supplementary Material) is accompanied by the $PM_{10}^{Tot}(\Delta t)$ increase (Fig. S2a of Supplementary Material). As will be seen later on, this occurrence has implications in terms of distribution of PM_{10} particles among the regions of the respiratory system.

The temporal evolution of aerosol number dose size distribution $D^{R}(d_{ae},t)$ on February 04th, 16th, 24th and 25th, in connection with the emission sources is described in Supplementary material (Fig. S8).

Fig. 6 shows the temporal trend of the percent contribution of $NPM_{x}^{R}(t)$ to $NPM_{10}^{R}(t)$ on 04th (a, b, c), 16th (d, e, f), 24th (g, h, i) and 25th (l, m, n). The relevant ranges of variation are summarized in Table 3. On number- based metric, during the four days examined, about 100% and more than 98% of $NPM_{10}^{R}(t)$ was respectively made of $NPM_{2.5}^{R}(t)$ and of $NPM_{1}^{R}(t)$.

On 16th (period 2 days) $NPM_{0.1}^{H}(t)\%$ varied from about 25% to 81% (Fig. 6d and Table 4). The highest contribution was estimated in the central part of the day, when fresh traffic related UFPs were more abundant than accumulation mode particles, that were predominant

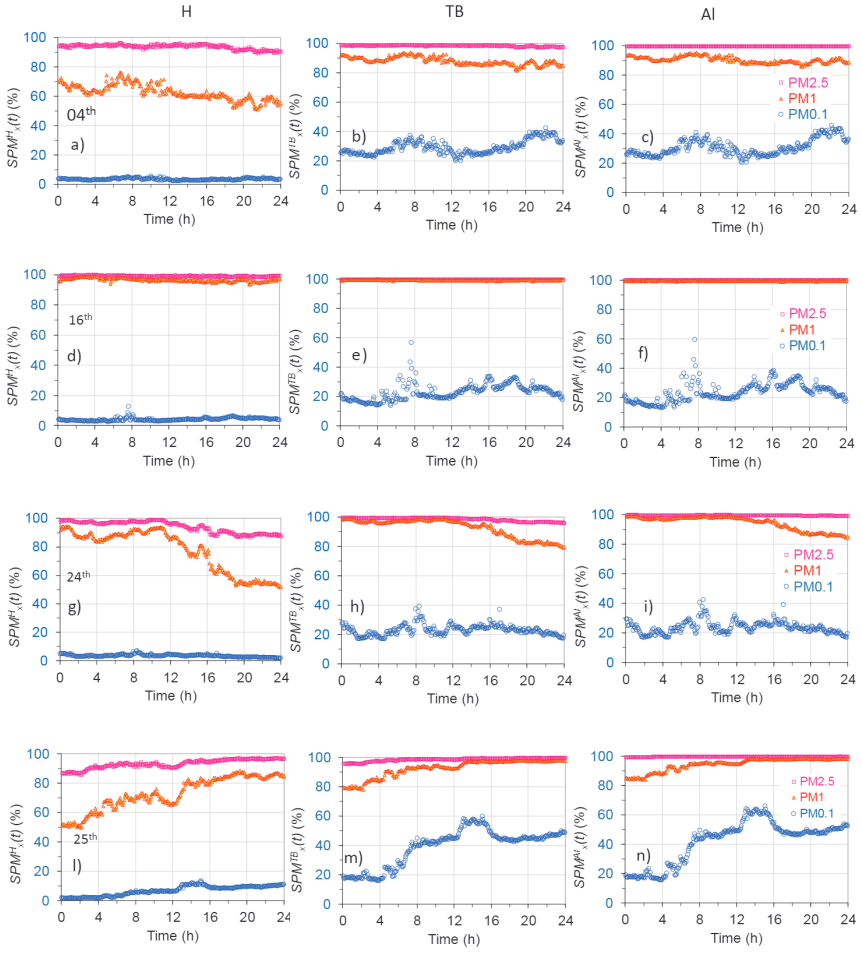

Fig. 4. Temporal trend of the percent contribution to total particle surface regional doses ($SPM_{10}^{R}(t)$) of the surface area based $SPM_x^R(t)$ (line colors represent x = 2.5 μm, 1 μm, 0.1 μm; column address R = H, TB, Al) on February 04th (a, b, c), 16th (d, e, f), 24th (g, h, i) and 25th (l, m, n). Each data point refers to a 5-min time interval.

Table 3
Ranges of variation of the percent contribution to total particle surface regional doses ($SPM_{10}^{R}(t)$) of the surface area based $SPM_x^R(t)$ (x = 2.5 μm, 1 μm, 0.1 μm), referred to a 5-min time interval, on February 04th, 16th, 24th and 25th.

Day	$SPM_{2.5}^{H}(t)$(%)	$SPM_{1}^{H}(t)$(%)	$SPM_{0.1}^{H}(t)$(%)	$SPM_{2.5}^{TB}(t)$(%)	$SPM_{1}^{TB}(t)$(%)	$SPM_{0.1}^{TB}(t)$(%)	$SPM_{2.5}^{Al}(t)$(%)	$SPM_{1}^{Al}(t)$(%)	$SPM_{0.1}^{Al}(t)$(%)
4th	89.3–96.5	51.1–76.2	1.9–5.5	97.3–99.2	81.6–94.1	19.5–42.2	99.7–99.9	85.7–95.4	19.9–45.5
16th	97.1–99.9	93.2–98.6	2.2–12.4	99.5–100	98.9–99.5	13.7–56.4	99.9–100	99.2–99.8	12.9–59.4
24th	86.4–98.9	51.8–94.4	1.4–6.8	96.0–99.8	79.2–98.9	16.6–39.0	99.5–100	84.5–99.1	16.5–42.2
25th	85.8–97.3	49.7–88.6	1.4–13.0	95.3–99.7	78.1–98.1	15.6–59.6	99.4–100	84.2–98.7	15.2–65.9

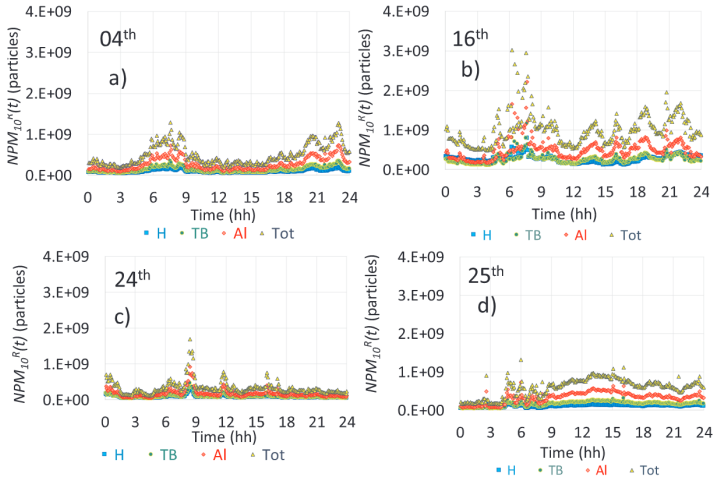

Fig. 5. Temporal evolution of total particle number ($NPM_{10}^{R}(t)$) regional doses (R = H, TB, Al, Tot) on 4th (a), 16th (b), 24th (c) and 25th (d). Each data point represents the dose deposited in a 5 min time interval.

during nocturnal hours, following the diurnal cycles outlined by Costabile et al. (2019). $NPM_{0.1}^{R}(t)$% increased in the TB end Al regions (Fig. 6e and f), because of the retention of coarser particle in the H region, it ranged respectively from about 62% to 97% and from 69% to 98%. On 04th the same modulation was observed. In addition, since accumulation mode particles were partially removed due to strong winds characterizing period 1 days, $NPM_{0.1}^{R}(t)$% was comparatively higher: 53–89%, 87–98% and 91–99% in the H, TB and Al region respectively. However at 2–6 pm it was lower on 04th than on 16th, amounting on average to 63%, 92%, 95% (04th) and 73%, 95%, 97% (16th), in the H, TB, Al region respectively, reflecting the increased contribution of sub-micrometer particle with size above UFP size range (sea salt aerosol). Moreover, even if slightly, $NPM_{2.5}^{H}(t)$% perceivably differed from $NPM_{1}^{H}(t)$% (< 1%), whereas on 16th the two fractions almost coincided.

Compared to mass metric, Saharan dust advection (period 3) to very minor extent affected also the number doses $NPM_{x}^{R}(t)$ from about 4 pm of 24th to about 8 am of 25th. Indeed, while on 16th (stable atmospheric condition and mainly local combustion sources) the difference between $NPM_{2.5}^{R}(t)$% and $NPM_{1}^{R}(t)$% was practically null, on 24th and 25th it was as high as 1.4% in the H region and as high as about 0.1% in the TB and Al regions (Fig. 6g–n).

Number doses give a representation of the dose distribution in the region of the respiratory system completely different from the mass metric. On mass basis, the highest doses were deposited in the H region, because this metric is mainly influenced by coarse particles that mainly derive from natural aerosol sources and or by dust re-suspension events. On the contrary, on number basis, doses are governed by UFPs and by particles of slightly greater size (less than about 0.2 μm), that deposit mainly in the alveolar region. The most important source of this kind of aerosol is combustion. Significantly the highest particle number and surface area doses estimated on 16th (Figs. 5b and 3b), correlated with independent observation on biological effects of air pollution recorded during the same period: i) the in vitro cellular-oxidative response in an epithelial cell line directly exposed to the ambient $PM_{1.5}$ (Gualtieri et al., 2018); ii) the aerosol oxidative potential (OP) determined by the 2,7-dichlorofluorescein (DCFH) assay (Manigrasso et al., 2020) induced by the soluble fraction of $PM_{2.5}$, including the insoluble non agglomerated UFPs; iii) the urinary excretion of 8-Oxo-7,8-dihydroguanosine, a biomarker of RNA oxidation (Costabile et al., 2019). Coherent with that, Bhargava et al. (2019) observed significantly higher levels of intracellular ROS and Nrf-2 in UFP exposed lymphocytes, than in control cells. The authors suggested that the increased levels of NF-kβ and of pro-inflammatory cytokines may activate an inflammatory loop, possibly triggering epigenetic alterations. They supported this interpretation by observing aberrant microRNA expression, DNA methylation and Histone modifications in UFP exposed cells. In the same direction is the study of Saffari et al. (2015) who emphasized the important oxidative contribution of particle with size below 0.25 μm, deriving from gasoline and diesel vehicles as well as from secondary organic aerosol.

In relation with that, the alveolar particle number and surface area doses are highly relevant from the health point of view. Alveoli separate the lung lumen from the blood stream by forming, by specific interactions among adjacent epithelial cells, underlying endothelial ones and the extracellular basement, the air-blood barrier (Patton and Byron, 2007). Here, due to their small size, UFPs may move by transcytosis across epithelial and endothelial cells, or due to cellular damages reducing the barrier efficiency of cells, into the blood and then lymph circulation, from where they can potentially reach sensitive sites and organs (Oberdörster et al., 2005). Within this context, it is crucial to consider that, due to the lack of suitable number concentrations datasets, traditionally great part of the epidemiological studies is based on aerosol mass concentrations, a metric that underrepresent the fraction of particles with highest oxidative activity.

3.2.4. *Olfactory bulb dosimetry*

UFPs deposited on the olfactory bulb with doses $D^{Olf}(t)$ (Fig. 7a and b) and $S^{Olf}(t)$ (Fig. 7c and d) that depended on both the intensity of combustion emission sources (traffic and biomass burning) and on the PBL mixing height modulation.

It is worth noting these doses do not take into account some particle properties, like solid/liquid state and in/solubility, which may be relevant in the translocation through the olfactory pathway.

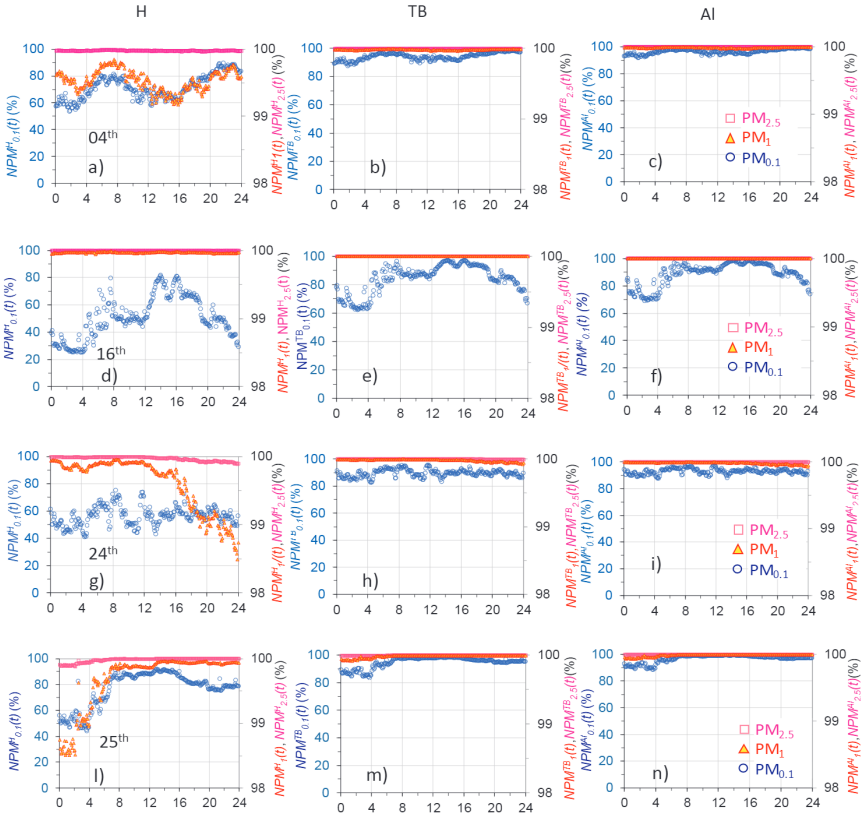

Fig. 6. Temporal trend of the percent contribution to total particle number regional doses ($NPM_{10}^{R}(t)$) of the number based $NPM_{x}^{R}(t)$ (line colors represent x = 2.5 μm, 1 μm, 0.1 μm; column address R = H, TB, Al) on February 04th (a, b, c), 16th (d, e, f), 24th (g, h, i) and 25th (l, m, n). Each data point refers to a 5-min time interval.

Overall higher doses were deposited on the 16th, in condition of atmospheric stability (on average 3.1×10^5 particles and 3.4×10^2 μm^2) than on the 4th (on average 2.2×10^5 particles and 1.7×10^2 μm^2) under advective conditions. Gobbi et al. (2019), based on lidar-ceilometer measurements, showed that the PBL mixing height generally decreases during the days before the Saharan dust advection, whereas it increases during the event. Coherently, lower doses were estimated on February 24th (on average 1.2×10^5 particles and 1.1×10^2 μm^2) and 25th (on average 2.6×10^5 particles and 2.2×10^2 μm^2) than on 16th, when the Saharan dust reached the ground. Moreover, the high wind speed characterizing such period concurred to the dispersion of surface aerosol.

As shown in Fig. 5a and b, in the central part of the day the temporal modulation was less pronounced on 4th, due to strong wind, than on

Table 4
Ranges of variation of the percent contribution to total particle number regional doses ($NPM_{10}^{R}(t)$) of the number based $NPM_{x}^{R}(t)$ (x = 2.5 μm, 1 μm, 0.1 μm), referred to a 5-min time interval, on February 04th, 16th, 24th and 25th.

Day	$NPM_{2.5}^{H}(t)$(%)	$NPM_{1}^{H}(t)$(%)	$NPM_{0.1}^{H}(t)$(%)	$NPM_{2.5}^{TB}(t)$(%)	$NPM_{1}^{TB}(t)$(%)	$NPM_{0.1}^{TB}(t)$(%)	$NPM_{2.5}^{Al}(t)$(%)	$NPM_{1}^{Al}(t)$(%)	$NPM_{0.1}^{Al}(t)$(%)
4th	99.9–100	99.2–99.8	53.2–89.7	100	99.9–100	87.4–98.4	100	100	91.3–99.0
16th	100	99.9–100	25.0–81.6	100	100	62.1–97.1	100	100	68.7–98.2
24th	99.9–100	98.5–99.9	40.9–75.0	100	99.9–100	82.5–95.4	100	99.9–100	87.4–97.1
25th	99.9–100	98.5–99.9	43.4–91.2	100	99.9–100	83.4–98.7	100	99.9–100	88.1–99.2

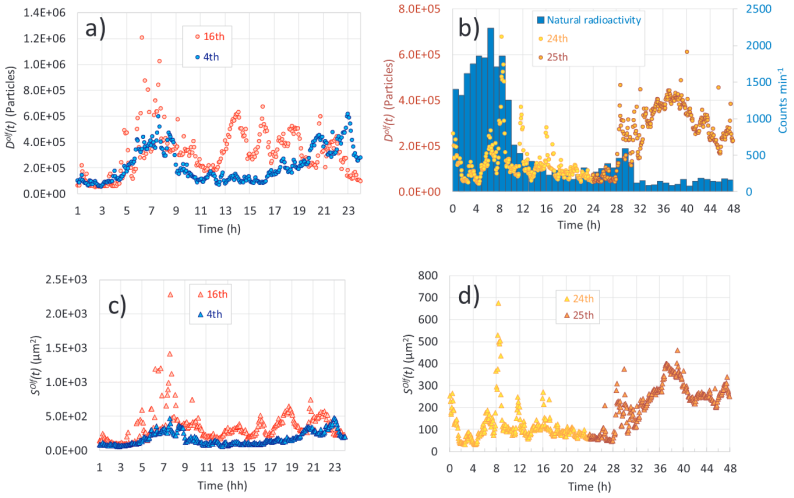

Fig. 7. Temporal trends of total particle number doses $D^{Olf}(t)$ (a) and surface area doses $S^{Olf}(t)$ (c) deposited on the olfactory bulb on February 4th and 16th. $D^{Olf}(t)$ and natural radioactivity on February 24th and 25th (b). $S^{Olf}(t)$ on February 24th and 25th (d).

16th. The same influence of traffic aerosol source and of PBL mixing height evolution was observed on 24th (Fig. 7b). Peak values were observed at the morning traffic rush hours and lower values when the PBL mixing height increased, as shown by the decreasing trend of natural radioactivity due to the short-life decay products of Radon. The same behaviour was retrieved on 25th in the first part of the day, until about 8 am, when the nucleation event (described in supplemental material) started.

PM air pollution has been recognized to play an important role in the development of neurodegenerative pathologies (Costa et al., 2017a). Exposure to traffic air pollution has been associated both to Parkinson's disease (PD) (Kasdagli et al. 2019; Shin et al., 2018) and to Alzheimer's disease (Calderón-Garcidueñas et al., 2004, 2008, 2012). Indeed, Calderón-Garcidueñas et al. (2008, 2012) found accumulation of Amyloid β-42 and α-Synuclein and hyper-phosphorylated tau in subjects exposed to high traffic air pollution. The authors reported that the hallmarks of Alzheimer's disease start from childhood and evolve with age, in relation with the exposure to combustion related nanoparticles, with carriers of Apolipoprotein E allele 4 (APOE4) being at higher risk (Calderón-Garcidueñas et al., 2008, 2018). Other studies have made associations between exposures to traffic air pollution and Autism Spectrum Disorders (ASDs) (Costa et al., 2017b).

Besides, olfactory dysfunction has been reported as an early clinical symptom in neurodegenerative disorders, such as Parkinson disease and Alzheimer's disease (Zou et al. 2016; Godoyet al., 2015) and has been observed in ASDs as well (Rozenkrantz, et al., 2015). On the one hand, in the studies of Cerza et al. (2018) in Rome and of Toro et al. (2019) in the Netherlands, the incidence of PD was not clearly related to the exposure to PM_{10}, $PM_{2.5}$, $PM_{2.5\text{-}10}$; on the other hand, UFPs have been retrieved in the olfactory bulb and the frontal cortical areas in the brain of highly exposed dogs and human beings (Calderón-Garcidueñas et al., 2008). Moreover, several studies demonstrated the translocation to brain through olfactory bulb and olfactory nerve of intranasally instilled (Oberdörster et al., 2005) and inhaled nanoparticles in experiment animals (Oberdörster et al., 2004; Balasubramanian et al., 2013). It is also worth observing that analysing the incidence of brain tumors in Montreal and Toronto, the study of Weichenthal et al (2019) reported for the first time a positive association between brain tumor incidence and UFPs (Hazard ratio = 1.133 for each 10^4 particle cm^{-3} increment of UFP concentration). All these studies point toward the relevance of correlating neurodegenerative and brain tumor pathologies with UFPs number and surface area concentrations, rather than with mass based PM_x concentrations and address the importance of estimating their doses deposited on the olfactory bulb, because they are candidate to possibly translocate to the brain. Considered in this perspective, the data here presented are particularly relevant, because the olfactory doses estimated are from UFP particles, with sizes almost similar to those found by Maher et al. (2016) in human brain samples. Here we determine these doses mainly from combustion derived nanoparticles, that have been shown to elicit a high oxidative response (Costabile et al., 2019; Bhargava et al., 2019). These UFP, after travelling along the olfactory bulb and reaching the brain, are potentially able to induce oxidative stress damages in neuronal cells and, noteworthy, oxidative stress is widely recognized to play an important role in the etiology of Alzheimer's disease (Cheignon et al., 2018).

4. Conclusions

An aerosol dosimetry study was carried out in the context of the "Carbonaceous Aerosol in Rome and Environs (CARE)" experiment, meant to improve the knowledge on the relationship between aerosol types and health effects. The study aimed to assess the dose levels of inhaled PM_{10}, its size distribution and allotment within the regions of the respiratory system, in relationship with the aerosol sources and atmospheric conditions.

These factors modulated the pollutant atmospheric concentrations on the time scales of one hour and of some days. Stable atmospheric conditions determined the accumulation of local anthropogenic fine mode aerosol, in the urban area studied represented by traffic and biomass burning emissions. Under such conditions, from 63% to 92% and from 80% to 99% of $PM_{10}^{H}(t)$ was made of $PM_{1}^{H}(t)$ and $PM_{2.5}^{H}(t)$, respectively. Such contributions increased passing from the H to the Al

region, where $PM_{10}^{R}(t)$, $PM_{2.5}^{R}(t)$ and $PM_{1}^{R}(t)$ almost coincided. Peculiar to the areas of Mediterranean basin is the advection of sea salt aerosol and of Saharan dust. Sea salt advection caused a contribution of coarse particles ($PM_{10}^{R}(t)$–$PM_{2.5}^{R}(t)$) to $PM_{10}^{R}(t)$ of 10–27% and 6–16%, deposited respectively in the H, TB regions whereas such contribution was negligible in the Al regions. Moreover, $PM_{2.5}^{R}(t)$ ceased being almost completely explained by $PM_{1}^{R}(t)$, the difference between the two fraction being about 45–61%, 31–48% and 26–44%, respectively in the H, TB and Al regions. During Saharan dust advection the contribution of coarse particles to $PM_{10}^{R}(t)$ was as high as 39% and 21% in the H and TB region and it was negligible in the Al region. $PM_{2.5}^{R}(t)$% markedly differed from$PM_{1}^{R}(t)$% even in the alveolar region, the difference between the two fractions being as high as 51%, 44% and 43%, respectively in the H, TB and Al regions. These data give a quantitative estimate of how the site of PM_{10} deposition within the respiratory system can considerably change, depending on the size distributions of enclosed particles. Therefore, even if its airborne concentrations happen to be the same, the relevant health effect may be different, given also the different chemical composition. Moreover, under some circumstances $PM_{2.5}^{R}(t)$, may include a significant contribution of particles deriving from natural sources (e.g. sea salt aerosol and Saharan dust) even in the alveolar region. These observations could explain why the strength of the associations between PM and health outcomes, reported in some studies, increases passing from considering PM_{10} to $PM_{2.5}$ and to PM_{1}. Therefore, on making associations between health endpoints and aerosol mass concentrations, the relevant coarse and fine fractions would be more properly adopted and the separation between them should be set at 1 μm, rather than at 2.5 μm.

During the morning rush hour, on average, 1.1×10^{10} particles, corresponding to 2.7×10^{4} ng and to 2.1×10^{8} μm^2 were, deposited in the respiratory system. On mass and surface area metric, particles more abundantly deposited in the H region, whereas on number metric, higher doses were estimated in the alveolar region. More than 98% of $NPM_{10}^{R}(t)$ in the H, TB and Al regions was represented by particles below 1 μm. The contribution of UFPs was relevant but did not fully explain $NPM_{1}^{R}(t)$ doses. This was due the distance of the measuring site from traffic roads, that allowed nucleation particles, abundantly emitted close to the vehicle tailpipes, to decay by impaction on surfaces or to grow by coagulation. This was also due to the contribution of biomass burning aerosol, that includes a relevant fraction of particles of size above the UFP size range. In periods of atmospheric stability and during nocturnal hours, when aged particles prevailed over UFPs and biomass burning sources were active, $NPM_{0.1}^{R}(t)$ was on average 29%, 67% and 73% of $NPM_{10}^{R}(t)$, respectively in the H, TB and Al regions. When the PBL mixing height increased, favouring the dispersion of aged larger particles, freshly emitted UFPs prevailed and $NPM_{0.1}^{R}(t)$ was on average 68%, 93%, 96%, respectively in the H, TB and Al regions. UFPs fully explained the dose of particles deposited on the olfactory bulb, that depended both on the intensity of the combustion sources and on and on meteorology (dispersion turbulence, PBL mixing height, precipitations) (Avino et al., 2003). $D^{Olf}(t)$ and $S^{Olf}(t)$ were respectively about 2.5-fold and 3.0-fold higher on a day of atmospheric stability than in condition of increased PBL vertical remixing. This fraction of particles is strongly underrepresented by the mass metric. The particle surface area and the number metrics would be more appropriate, rather than PM_x mass concentrations, to correlate neurodegenerative pathologies with aerosol pollution, also in consideration of the high oxidative activity of these particles.

CRediT authorship contribution statement

Maurizio Manigrasso: Conceptualization, Methodology, Formal analysis, Writing - original draft, Project administration. **Francesca Costabile:** Validation, Investigation, Resources, Data curation. **Luca Di Liberto:** Investigation. **Gian Paolo Gobbi:** Supervision, Funding acquisition. **Maurizio Gualtieri:** Investigation, Resources. **Gabriele Zanini:** Investigation, Visualization. **Pasquale Avino:** Methodology, Supervision, Writing - review & editing.

Declaration of Competing Interest

The authors declare that they have no known competing financial interests or personal relationships that could have appeared to influence the work reported in this paper.

Acknowledgements

The CARE experiment was organized by ISAC CNR and realized with the logistical support of the Councillor for environmental sustainability of “Roma Capitale”. We wish to thank Giuseppina Montanari, Pasquale Pelusi, Giuseppe Lanzi, Stefano Cicerani, Silvano Simoni, Vincenzo Cimaglia, Massimo Rascioni, Daniele Rocchi, Eugenio Donato. The authors would also like to thank all research groups that co-financed activities required for their participation in the CARE experiment, and in particular, all the scientists and technicians involved, namely, Honey Alas,Fulvio Amato, Stefania Argentini, Michaela Aufderheide, Massimo Berico, Francesca Barnaba, Vera Bernardoni, Riccardo Biondi, Giulia Calzolai, Silvia Canepari, Giampietro Casasanta, Spartaco Ciampichetti Luisella Ciancarella, Alessandro Conidi, Eugenia Cordelli, Antonio Di Ianni, Maria Cristina Facchini, Andrea Facci, Daniele Frasca, Stefania Gilardoni, Teresa La Torretta, Franco Lucarelli, Antonella Malaguti, Niklas Mohle, Mauro Montagnoli, Silvia Nava, Francesca Pacchierotti, Elio Padoan, Cinzia Perrino, Igor Petenko, Xavier Querol, Giuseppe Raschella, Giulia Simonetti, Milena Stracquadanio, Giovanna Tranfo, Stefano Ubertini, Gianluigi Valli, Sara Valentini, Roberta Vecchi, Francesca Volpi, Kay Weinhold, Alfred Wiedensohler..

The authors gratefully thank ARA for making available MPPD version 3.01 and ARPA Lazio for publically making available ozone data.

Funding

This research did not receive any specific grant from funding agencies in the public, commercial, or not-for-profit sectors.

Appendix A. Supplementary material

Supplementary data to this article can be found online at https://doi.org/10.1016/j.envint.2020.105714.

References

Akima, H., 1970. A new method of interpolation and smooth curve fitting based on local procedures. J. Assoc. Omput. Mach. 17, 589–602.

Alas, H.D.C., Weinhold, K., Costabile, F., Di Ianni, A., Müller, T., Pfeifer, S., Di Liberto, L., Turner, J.R., Wiedensohler, A., 2019. Methodology for high-quality mobile measurement with focus on black carbon and particle mass concentrations. Atmos. Meas. Tech. 12, 4697–4712.

Albinet, A., Leoz-Garziandia, E., Budzinski, H., Villenave, E., Jaffrezo, J.-L., 2008. Nitrated and oxygenated derivatives of polycyclic aromatic hydrocarbons in the ambient air of two French alpine valleys Part 2: particle size distribution. Atmos. Environ. 42, 55–64.

Albuquerque, P.C., Gomes, J.F., Bordado, J.C., 2012. Assessment of exposure to airborne ultrafine particles in the urban environment of Lisbon, Portugal. J. Air Waste Manage. Assoc. 62, 373–380.

Asgharian, B., Hofmann, W., Bergmann, R., 2001. Particle deposition in a multiple-path model of the human lung. Aerosol Sci. Technol. 34, 332–339.

Avino, P., Brocco, D., Lepore, L., Ventrone, I., 2000. Distribution of elemental carbon (EC) and organic carbon (OC) in the atmospheric aerosol particles of Rome. J. Aerosol Sci. 31, S364–S365.

Avino, P., Brocco, D., Cecinato, A., Lepore, L., Balducci, C., 2002. Carbonaceous components in atmospheric aerosol: measurement procedures and characterization. Ann. Chim. 92, 333–341.

Avino, P., Brocco, D., Lepore, L., Pareti, S., 2003. Interpretation of atmospheric pollution phenomena in relationship with the vertical atmospheric remixing by means of natural radioactivity measurements (radon) of particulate matter. Ann. Chim. 93, 589–594.

Avino, P., Manigrasso, M., 2008. Ten-year measurements of gaseous pollutants in urban air by an open-path analyzer. Atmos. Environ. 42, 4138–4148.

Avino, P., Protano, C., Vitali, M., Manigrasso, M, 2016. Benchmark study on fine-mode aerosol in a big urban area and relevant doses deposited in the human respiratory tract. Environ. Pollut. 216, 530–537. https://doi.org/10.1016/j.envpol.2016.06.005.

Babadjouni, R.M., Hodis, D.M., Radwanski, R., Durazo, R., Patel, A., Liu, Q., Mack, W.J., 2017. Clinical effects of air pollution on the central nervous system; a review. J. Clin. Neurosci. 43, 16–24.

Balasubramanian, S.K., Poh, K., Ong, C., Kreyling, W.G., Ong, W., Yu, L.E., 2013. The effect of primary particle size on biodistribution of inhaled gold nanoagglomerates. Biomaterials 34, 5439–5452.

Bhargava, A., Shukla, A., Bunkar, N., Shandilya, R., Lodhi, L., Kumari, R., Gupta, P., Rahman, A., Chaudhury, K., Tiwari, R., Goryacheva, I.Y., Mishra, P.K., 2019. Exposure to ultrafine particulate matter induces NF-κβ mediated epigenetic modifications. Environ. Pollut. 252, 39–50.

Brunekreef, B., Forsberg, B., 2005. Epidemiological evidence of effects of coarse airborne particles on health. Eur. Respir. J. 26, 309–318.

Calderón-Garcidueñas, L., Reed, W., Maronpot, R.R., Henríquez-Roldán, C., Delgado-Chavez, R., Calderón-Garcidueñas, A., Dragustinovis, I., Franco-Lira, M., Aragón-Flores, M., Solt, A.C., Altenburg, M., Torres-Jardón, R., Swenberg, J.A., 2004. Brain inflammation and Alzheimer's-like pathology in individuals exposed to severe air pollution. Toxicol. Pathol. 32, 650–658.

Calderón-Garcidueñas, L., Solt, A.C., Henríquez-Roldán, C., Torres-Jardón, R., Nuse, B., Herritt, L., Villarreal-Calderón, R., Osnaya, N., Stone, I., García, R., Brooks, D.M., González-Maciel, A., Reynoso-Robles, R., Delgado-Chávez, R., Reed, W., 2008. Long-term air pollution exposure is associated with neuroinflammation, an altered innate immune response, disruption of the blood-brain barrier, ultrafine particulate deposition, and accumulation of amyloid beta-42 and alpha-synuclein in children and young adults. Toxicol. Pathol. 36, 289–310.

Calderón-Garcidueñas, L., Kavanaugh, M., Block, M., D'Angiulli, A., Delgado-Chávez, R., Torres-Jardón, R., González-Maciel, A., Reynoso-Robles, R., Osnaya, N., Villarreal-Calderon, R., Guo, R., Hua, Z., Zhu, H., Perry, G., Diaz, P., 2012. Neuroinflammation, hyperphosphorylated tau, diffuse amyloid plaques, and down-regulation of the cellular prion protein in air pollution exposed children and young adults. J. Alzheimers Dis. 28, 93–107.

Calderón-Garcidueñas, L., Gónzalez-Angélica, M., Reynoso-Robles, R., Delgado-Chávez, R., Mukherjee, P.S., Kulesza, R.J., Torres-Jardón, R., Ávila-Ramírez, J., Villarreal-Ríos, R., 2018. Hallmarks of Alzheimer disease are evolving relentlessly in Metropolitan Mexico City infants, children and young adults. APOE4 carriers have higher suicide risk and higher odds of reaching NFT stage V at ≤40 years of age. Environ. Res. 164, 475–487.

Cerza, F., Renzi, M., Agabiti, N., Marino, C., Gariazzo, C., Davoli, M., Michelozzi, P., Forastiere, F., Cesaroni, G., 2018. Residential exposure to air pollution and incidence of Parkinson's disease in a large metropolitan cohort. Environ. Epidemiol. 2, 3023.

Cheignon, C., Tomas, M., Bonnefont-Rousselot, D., Faller, P., Hureau, C., Collin, F., 2018. Oxidative stress and the amyloid beta peptide in Alzheimer's disease. Redox Biol. 14, 450–464.

Chen, R., Li, Y., Ma, Y., Pan, G., Zeng, G., Xu, X., Chen, B., Kan, H., 2011. Coarse particles and mortality in three Chinese cities: the China air pollution and health effects study (CAPES). Sci. Total Environ. 409, 4934–4938.

Chen, H., Kwong, J.C., Copes, R., Tu, K., Villeneuve, P., van Donkelaar, A., Hystad, P., Martin, R.V., Murray, B., Jessiman, B., Wilton, A.S., Kopp, A., Burnett, R.Y., 2017. Living near major roads and the incidence of dementia, Parkinson's disease, and multiple sclerosis: a population-based cohort study. Lancet 389, 718–726.

Costa, L.G., Cole, T.B., Coburn, J., Chang, Y.C., Dao, K., Roque, P., 2014. Neurotoxicants are in the air: convergence of human, animal, and in vitro studies on the effects of air pollution on the brain. Biomed. Res. Int. 2014, 736385.

Costa, L.G., Cole, T.B., Coburn, J., Chang, Y.C., Dao, K., Roque, P., 2017a. Neurotoxicity of traffic-related air pollution. Neurotoxicology 59, 133–139.

Costa, L.G., Chang, Y.-C., Cole, T.B., 2017b. Developmental neurotoxicity of traffic-related air pollution: focus on autism. Curr. Environ. Health Rep. 4, 156–165.

Costabile, F., Alas, H., Aufderheide, M., Avino, P., Amato, F., Argentini, S., Barnaba, F., Berico, M., Bernardoni, V., Biondi, R., Calzolai, G., Canepari, S., Casasanta, G., Ciampichetti, S., Conidi, A., Cordelli, E., Ianni, A.D., Liberto, L.D., Facchini, M.C., Facci, A., Frasca, D., Gilardoni, S., Grollino, M.G., Gualtieri, M., Lucarelli, F., Malaguti, A., Manigrasso, M., Montagnoli, M., Nava, S., Padoan, E., Perrino, C., Petralia, E., Petenko, I., Querol, X., Simonetti, G., Tranfo, G., Ubertini, S., Valli, G., Valentini, S., Vecchi, R., Volpi, F., Weinhold, K., Wiedensholer, A., Zanini, G., Gobbi, G.P., 2017. First results of the "Carbonaceous Aerosol in Rome and Environs (CARE)" Experiment: beyond current standards for PM_{10}. Atmosphere 8 art. 249.

Costabile, F., Gualtieri, M., Canepari, S., Tranfo, G., Consales, C., Grollino, M.G., Paci, E., Petralia, E., Pigini, D., Simonetti, G., 2019. Evidence of association between aerosol properties and in-vitro cellular oxidative response to PM_1, oxidative potential of $PM_{2.5}$, a biomarker of RNA oxidation, and its dependency on combustion sources. Atmos. Environ. 213, 444–455.

DeCarlo, P.F., Slowik, J.G., Worsnop, D.R., Davidovits, P., Jimenez, J.L., 2004. Particle morphology and density characterization by combined mobility and aerodynamic diameter measurements. Part 1: theory. Aerosol Sci. Technol. 38, 1185–1205.

Di Filippo, P., Pomata, D., Riccardi, C., Buiarelli, F., Gallo, V., 2015. Oxygenated polycyclic aromatic hydrocarbons in size-segregated urban aerosol. J. Aerosol. Sci. 87, 126–134.

Dockery, D.W., Pope, C.A., Xu, X., Spengler, J.D., Ware, J.H., Fay, M.E., Ferris Jr, B.G., Speizer, F.E., 1993. An association between air pollution and mortality in six U.S. cities. N. Engl. J. Med. 329, 1753–1759.

Donaldson, K., Stone, V., Clouter, A., Renwick, L., MacNee, W., 2001. Ultrafine particles. Occup. Environ. Med. 58, 211–216.

Fang, T., Guo, H., Zeng, L., Verma, V., Nenes, A., Weber, R.J., 2017. Highly acidic ambient particles, soluble metals and oxidative potential: a link between sulfate and aerosol toxicity. Environ. Sci. Technol. 51, 2611–2620.

Fiorello, A., Amato, F., Bernardoni, V., Calzolai, G., Canepari, S., Costabile, F., Di Liberto, L., Gualtieri, M., Lucarelli, F., Nava, S., Perrino, C., Petralia, E., Valentini, S., Valli, G., Vecchi, R., 2020. Gaining knowledge on source contribution to aerosol optical absorption properties and organics by receptor modelling. Atmos. Environ (submitted for publication).

Gobbi, G.P., Angelini, F., Barnaba, F., Costabile, F., Baldasano, J.M., Basart, S., Sozzi, R., Bolignano, A., 2013. Changes in particulate matter physical properties during Saharan advections over Rome (Italy): a four-year study, 2001–2004. Atmos. Chem. Phys. 13, 7395–7404.

Gobbi, G.P., Barnaba, F., Di Liberto, L., Bolignano, A., Lucarelli, F., Nava, S., Perrino, C., Pietrodangelo, A., Basart, S., Costabile, F., Dionisi, D., Rizza, U., Canepari, S., Sozzi, R., Morelli, M., Manigrasso, M., Drewnick, F., Struckmeier, C., Poenitz, K., Wille, H., 2019. An inclusive view of Saharan dust advections to Italy and the Central Mediterranean. Atmos. Environ. 201, 242–256.

Godoy, M.D., Voegels, R.L., Pinna, F. de R., Imamura, R., Farfel, J.M., 2015. Olfaction in neurologic and neurodegenerative diseases: a literature review. Int. Arch. Otorhinolaryngol. 19, 176–179.

Gualtieri, M., Grollino, M.G., Consales, C., Costabile, F., Manigrasso, M., Avino, P., Aufderheide, M., Cordelli, E., Di Liberto, L., Petralia, E., Raschellà, G., Stracquadanio, M., Wiedensohler, A., Pacchierotti, F., Zanini, G., 2018. Is it the time to study air pollution effects under environmental conditions? A case study to support the shift of in vitro toxicology from the bench to the field. Chemosphere 207, 552–564.

Hennig, F., Quass, U., Hellack, B., Küpper, M., Kuhlbusch, T.A.J., Stafoggia, M., Hoffmann, B., 2018. Ultrafine and fine particle number and surface area concentrations and daily cause-specific mortality in the Ruhr Area, Germany, 2009–2014. Environ. Health Perspect. 126 art. 027008.

Hinds, W.C., 1999. Aerosol Technology, second ed. Wiley, New York, NY, USA ISBN: 978-0-471-19410-1.

Hoek, G., Pattenden, S., Willers, S., Antova, T., Fabianova, E., Braun-Fahrländer, C., Forastiere, F., Gehring, U., Luttmann-Gibson, H., Grize, L., Heinrich, J., Houthuijs, D., Janssen, N., Katsnelson, B., Kosheleva, A., Moshammer, H., Neuberger, M., Privalova, L., Rudnai, P., Speizer, F., Slachtova, H., Tomaskova, H., Zlotkowska, R., Fletcher, T., 2012. PM10, and children's respiratory symptoms and lung function in the PATY study. Eur. Respir. J. 40, 538–547.

Hu, M., Peng, J., Sun, K., Yue, D., Guo, S., Wiedensohler, A., Wu, Z., 2012. Estimation of size-resolved ambient particle density based on the measurement of aerosol number, mass, and chemical size distributions in the winter in Beijing. Environ. Sci. Technol. 46, 9941–9947.

Hussain, S., Boland, S., Baeza-Squiban, A., Hamel, R., Thomassen, L.C., Martens, J.A., Billon-Galland, M.A., Fleury-Feith, J., Moisan, F., Pairon, J.C., Marano, F., 2009. Oxidative stress and proinflammatory effects of carbon black and titanium dioxide nanoparticles: role of particle surface area and internalized amount. Toxicology 260, 142–149.

IARC, 2013. Outdoor Air Pollution IARC Monographs: IARC Monographs on the Evaluation of Carcinogenic Risks to Humans. International Agency for Research on Cancer, Lyon, France.

ICRP, 1994. Human respiratory tract model for radiological protection. ICRP Publication 66. Ann. ICRP 24, 1–3.

Kasdagli, M.-I., Katsouyanni, K., Dimakopoulou, K., Samoli, E., 2019. Air pollution and Parkinson's disease: a systematic review and meta-analysis up to 2018. Int. J. Hyg. Environ. Heal. 222, 402–409.

Khlystov, A., Stanier, C., Pandis, S.N., 2004. An algorithm for combining electrical mobility and aerodynamic size distributions data when measuring ambient aerosol special issue of aerosol science and technology on findings from the fine particulate matter supersites program. Aerosol. Sci. Technol. 38, 229–238.

Lepeule, J., Laden, F., Dockery, D., Schwartz, J., 2012. Chronic exposure to fine particles and mortality: an extended follow-up of the Harvard Six Cities study from 1974 to 2009. Environ. Health Perspect. 120, 965–970.

Levy, J.I., Hammitt, J.K., Spengler, J.D., 2000. Estimating the mortality impacts of particulate matter: what can be learned from between-study variability? Environ. Health Perspect. 108, 109–117.

Li, N., Sioutas, C., Cho, A., Schmitz, D., Misra, C., Sempf, J., Wang, M., Oberley, T., Froines, J., Nel, A., 2003. Ultrafine particulate pollutants induce oxidative stress and mitochondrial damage. Environ. Health Perspect. 111, 455–460.

Lin, H., Tao, J., Du, Y., Liu, T., Qian, Z., Tian, L., Di, Q., Rutherford, S., Guo, L., Zeng, W., Xiao, J., Li, X., He, Z., Xu, Y., Ma, W., 2016. Particle size and chemical constituents of ambient particulate pollution associated with cardiovascular mortality in Guangzhou. China. Environ. Pollut. 208, 758–766.

Maher, B.A., Ahmed, I.A.M., Karloukovski, V., MacLaren, D.A., Foulds, P.G., Allsop, D., Mann, D.M.A., Torres-Jardón, R., Calderon-Garciduenas, L., 2016. Magnetite pollution nanoparticles in the human brain. P. Natl. Acad. Sci. USA 113, 10797–10801.

Malig, B.J., Ostro, B.D., 2009. Coarse particles and mortality: evidence from a multi-city study in California. Occup. Environ. Med. 66, 832–839.

Mallone, S., Stafoggia, M., Faustini, A., Gobbi, G.P., Marconi, A., Forastiere, F., 2011. Saharan dust and associations between particulate matter and daily mortality in Rome, Italy. Environ. Health Perspect. 119, 1409–1414.

Manigrasso, M., Febo, A., Guglielmi, F., Ciambottini, V., Avino, P., 2012. Relevance of aerosol size spectrum analysis as support to qualitative source apportionment studies. Environ. Pollut. 170, 43–51.

Manigrasso, M., Simonetti, G., Astolfi, M.L., Perrino, C., Canepari, S., Protano, C., Antonucci, A., Avino, P., Vitali, M., 2020. Oxidative potential associated with urban aerosol deposited into the respiratory system and relevant elemental and ionic fraction contributions. Atmosphere 11, 6. https://doi.org/10.3390/

ATMOS11010006.
Manigrasso, M., Vernale, C., Avino, P., 2017. Traffic aerosol lobar doses deposited in the human respiratory system. Environ. Sci. Pollut. Res. Int. 24, 13866–13873. https://doi.org/10.1007/s11356-015-5666-1.
Manigrasso, M., Vitali, M., Protano, C., Avino, P., 2018. Ultrafine particles in domestic environments: regional doses deposited in the human respiratory system. Environ. Int. 118, 134–145.
Manigrasso, M., Protano, C., Vitali, M., Avino, P., 2019a. Where do ultrafine particles and nano-sized particles come from? J. Alzheimer's Dis. 68, 1371–1390.
Manigrasso, M., Protano, C., Astolfi, M.L., Massimi, L., Avino, P., Vitali, M., Canepari, S., 2019b. Evidences of copper nanoparticle exposure in indoor environments: long-term assessment, high-resolution field emission scanning electron microscopy evaluation, in silico respiratory dosimetry study and possible health implications. Sci. Total Environ. 653, 1192–1203.
Martuzzi, M., Galassi, C., Ostro, B., Forastiere, F., Bertollini, R., 2002. Health impact assessment of air pollution in the eight major Italian cities. World Health Organization, EURO/02/5040650. ISBN 92-890-1085-1. Available at http://www.euro.who.int/_data/assets/pdf_file/0013/91111/E75492.pdf. Last access on September 2019.
Massling, A., Stock, M., Wehner, B., Wu, Z.J., Hu, M., Brüggemann, E., Gnauk, T., Herrmann, H., Wiedensohler, A., 2009. Size segregated water uptake of the urban submicrometer aerosol in Beijing. Atmos. Environ. 43, 1578–1589.
Meng, X., Ma, Y., Chen, R., Zhou, Z., Chen, B., Kan, H., 2013. Size-fractionated particle number concentrations and daily mortality in a Chinese city. Environ. Health Perspect. 121, 1174–1178.
Nava, S., Calzolai, G., Chiari, M., Lucarelli, F., Costabile, F., Di Liberto, L., Gobbi, G.P., Bernardoni, V., Valentini, S., Valli, G., Vecchi, R., 2018. Studio del particolato atmosferico urbano con alta risoluzione temporale: risultati delle analisi orarie PIXE e termo-ottiche del progetto CARE. In: Proc. VIII Nat. Congr. Atmospheric Particulate Matter PM2018, May 23-25, Matera, Italy, pp. 127 ISBN: 978-88-942135-1-5 (In Italian).
Nel, A., Xia, T., Mädler, L., Li, N., 2006. Toxic potential of materials at the nanolevel. Science 311, 622–627.
Oberdörster, G., Sharp, Z., Atudorei, V., Elder, A., Gelein, R., Kreyling, W., Cox, C., 2004. Translocation of inhaled ultra-fine particles to the brain. Inhal. Toxicol. 16, 437–445.
Oberdörster, G., Oberdörster, E., Oberdörster, J., 2005. Nanotoxicology: an emerging discipline evolving from studies of ultrafine particles. Environ. Health Perspect. 113, 823–839.
Patton, J.S., Byron, P.R., 2007. Inhaling medicines: delivering drugs to the body through the lungs. Nat. Rev. Drug Discov. 6, 67–74.
Peng, R.D., Chang, H.H., Bell, M.L., McDermott, A., Zeger, S.L., Samet, J.M., Dominici, F., 2008. Coarse particulate matter air pollution and hospital admissions for cardiovascular and respiratory diseases among Medicare patients. JAMA 299, 2172–2179.
Perez, L., Tobias, A., Querol, X., Künzli, N., Pey, J., Alastuey, A., Viana, M., Valero, N., González-Cabré, M., Sunyer, J., 2008. Coarse particles from Saharan dust and daily mortality. Epidemiology 19, 800–807.
Pope III, C.A., Burnett III, R.T., Thun, M.J., 2002. Lung cancer, cardiopulmonary mortality, and long-term exposure to fine particulate air pollution. JAMA 287, 1132–1141.
Pope III, C.A., Rodermund, D.L., Gee, M.M., 2007. Mortality effects of a copper smelter strike and reduced ambient sulfate particulate matter air pollution. Environ. Health Perspect. 115, 679–683.
Querol, X., Pey, J., Pandolfi, M., Alastuey, A., Cusack, M., Pérez, N., Moreno, T., Viana, M., Mihalopoulos, N., Kallos, G., Kleanthous, S., 2009. African dust contributions to mean ambient PM10 mass-levels across the Mediterranean Basin. Atmos. Environ. 43, 4266–4277.
Romeo, E., De Sario, M., Forastiere, F., Compagnucci, P., Stafoggia, M., Bergamaschi, A., Perucci, C.A., 2006. PM 10 exposure and asthma exacerbations in pediatric age: a meta-analysis of panel and time-series studies. Epidemiol. Prev. 30, 245–254.
Rozenkrantz, L., Zachor, D., Heller, I., Plotkin, A., Weissbrod, A., Snitz, K., Secundo, L., Sobel, N., 2015. A mechanistic link between olfaction and autism spectrum disorder. Curr. Biol. 25, 1904–1910.
Saffari, A., Hasheminassab, S., Wang, D., Shafe, M.M., Schauer, J.J., Sioutas, C., 2015. Impact of primary and secondary organic sources on the oxidative potential of quasi-ultrafine particles ($PM_{0.25}$) at three contrasting locations in the Los Angeles Basin. Atmos. Environ. 120, 286–296.
Salvadora, P., Molero, F., Fernandez, A.J., Tobías, A., Pandolfi, M., Gómez-Moreno, F.J., Barreiro, M., Pérez, N., Marco, I.M., Revuelta, M.A., Querol, X., Artiñano, B., 2019. Synergistic effect of the occurrence of African dust outbreaks on atmospheric pollutant levels in the Madrid metropolitan area. Atmos. Res. 226, 208–218.
Sandström, T., Nowak, D., van Bree, L., 2005. Health effects of coarse particles in ambient air: messages for research and decision-making. Eur. Respir. J. 26, 187–188.
Shaddick, G., Thomas, M.L., Amini, H., Broday, D., Cohen, A., Frostad, J., Green, A., Gumy, S., Liu, Y., Martin, R.V., Pruss-Ustun, A., Simpson, D., van Donkelaar, A., Brauer, M., 2018. Data integration for the assessment of population exposure to ambient air pollution for global burden of disease assessment. Environ. Sci. Technol. 52, 9069–9078.
Shi, L., Xu, X., Dou, X.Y., Zhao, X., 2014. The research progress of heavy metals in $PM_{2.5}$. Adv. Mater. Res. 955, 1397–1404.
Shin, S., Burnett, R.T., Kwong, J.C., Hystad, P., Van Donkelaar, A., Brook, J.R., Copes, R., Tu, K., Goldberg, M.S., Villeneuve, P.J., Martin, R.V., Murray, B.J., Wilton, A.S., Kopp, A., Chen, H., 2018. Effects of ambient air pollution on incident Parkinson's disease in Ontario, 2001 to 2013: a population-based cohort study. Int. J. Epidemiol. 47, 2038–2048.
Smith, K.R., Jerrett, M., Anderson, H.R., Burnett, R.T., Stone, V., Derwent, R., Atkinson, R.W., Cohen, A., Shonkoff, S.B., Krewski, D., Pope III, C.A., Thun, M.J., Thurston, G., 2009. Public health benefits of strategies to reduce greenhouse-gas emissions: health implications of short-lived greenhouse pollutants. Lancet 374, 2091–2103.
Stock, M., Cheng, Y.F., Birmili, W., Massling, A., Wehner, B., Müuller, T., Leinert, S., Kalivitis, N., Mihalopoulos, N., Wiedensohler, A., 2011. Hygroscopic properties of atmospheric aerosol particles over the Eastern Mediterranean: implications for regional direct radiative forcing under clean and polluted conditions. Atmos. Chem. Phys. 11, 4251–4271.
Swietlicki, E., Hansson, H.-C., Hämeri, K., Svenningsson, B., Massling, A., Mcfiggans, G., Mcmurry, P.H., Petäjä, T., Tunved, P., Gysel, M., Topping, D., Weingartner, E., Baltensperger, U., Rissler, J., Wiedensohler, A., Kulmala, M., 2008. Hygroscopic properties of submicrometer atmospheric aerosol particles measured with H-TDMA instruments in various environments – a review. Tellus 60B, 432–469.
Targino, A.C., Gibson, M.D., Krecl, P., Rodrigues, M.V.C., dos Santos, M.M., Corrêa, M.P., 2016. Hotspots of black carbon and $PM_{2.5}$ in an urban area and relationships to traffic characteristics. Environ. Pollut. 218, 475–486.
Toro, R., Downward, G.S., van der Mark, M., Brouwer, M., Huss, A., Peters, S., Hoek, G., Nijssen, P., Mulleners, W.M., Sas, A., van Laar, T., Kromhout, H., Vermeulen, R., 2019. Parkinson's disease and long-term exposure to outdoor air pollution: a matched case-control study in the Netherlands. Environ. Inter. 129, 28–34.
Valentini, S., Barnaba, F., Bernardoni, V., Calzolai, G., Costabile, F., Di Liberto, L., Forello, A.C., Gobbi, G.P., Gualtieri, M., Lucarelli, F., et al., 2020. Classifying aerosol particles through the combination of optical and physical-chemical properties: Results from a wintertime campaign in Rome (Italy). Atmos. Res. 235.
Viidanoja, J., Sillanpää, M., Laakia, J., Kerminen, V.-M., Hillamo, R., Aarnio, P., Koskentalo, T., 2002. Organic and black carbon in PM2.5 and PM10: 1 year of data from an urban site in Helsinki. Finland. Atmos. Environ. 36, 3183–3193.
Vu, T.V., Delgado-Saborit, J.M., Harrison, R.M., 2015. A review of hygroscopic growth factors of submicron aerosols from different sources and its implication for calculation of lung deposition efficiency of ambient aerosols. Air Qual. Atmos. Health 8, 429–440.
Weichenthal, S., Olaniyan, T., Christidis, T., Lavigne, E., Hatzopoulou, M., Van Ryswyk, K., Tjepkema, M., Burnett, R., 2019. Within-city spatial variations in ambient ultrafine particle concentrations and incident brain tumors in adults. Epidemiology. Nov 6. doi: 10.1097/EDE.0000000000001137. [in press].
Wellenius, G.A., Schwartz, J., Mittleman, M.A., 2005. Air pollution and hospital admissions for ischemic and hemorrhagic stroke among medicare beneficiaries. Stroke 36, 2549–2553.
WHO, 2013. Health Effects of Particulate Matter. WHO Regional Office for Europe, Copenhagen, Denmark.
Wiedensohler, A., Birmili, W., Nowak, A., Sonntag, A., Weinhold, K., Merkel, M., Wehner, B., Tuch, T., Pfeifer, S., Fiebig, M., Fjäraa, A.M., Asmi, E., Sellegri, K., Depuy, R., Venzac, H., Villani, P., Laj, P., Aalto, P., Ogren, J.A., Swietlicki, E., Williams, P., Roldin, P., Quincey, P., Hüglin, C., Fierz-Schmidhauser, R., Gysel, M., Weingartner, E., Riccobono, F., Santos, S., Grüning, C., Faloon, K., Beddows, D., Harrison, R., Monahan, C., Jennings, S.G., O'Dowd, C.D., Marinoni, A., Horn, H.-G., Keck Jiang, L.J., Scheckman, P.H., McMurry, Z., Deng, C., Zhao, S., Moerman, M., Henzing, B., de Leeuw, G., Löschau, G., Bastian, S., 2012. Mobility particle size spectrometers: Harmonization of technical standards and data structure to facilitate high quality long-term observations of atmospheric particle number size distributions. Atmos. Meas. Tech. 5, 657–685.
Xia, T., Kovochich, M., Liong, M., Mädler, L., Gilbert, B., Shi, H., Yeh, J.I., Zink, J.I., Nel, A.E., 2008. Comparison of themechanismof toxicity of zinc oxide and ceriumoxide nanoparticles based on dissolution and oxidative stress properties. ACS Nano 2, 2121–2134.
Ye, X., Tang, C., Yin, Z., Chen, J., Ma, Z., Kong, L., Yang, X., Gao, W., Geng, F., 2013. Hygroscopic growth of urban aerosol particles during the 2009 Mirage-Shanghai Campaign. Atmos. Environ. 64, 263–269.
Zanobetti, A., Schwartz, J., 2009. The effect of fine and coarse particulate air pollution on mortality: a National analysis. Environ. Health Perspect. 117, 898–903.
Zhu, X., Hondroulis, E., Liu, W., Li, C.Z., 2013. Biosensing approaches for rapid genotoxicity and cytotoxicity assays upon nanomaterial exposure. Small 9, 1821–1830.
Zou, Y.-M., Lu, D., Liu, L.-P., Zhang, H.-H., Zhou, Y.-Y., 2016. Olfactory dysfunction in Alzheimer's disease. Neuropsych. Dis. Treat. 12, 869–875.